CHAPTER ONE

(1.1) INTRODUCTION

Spectrometers are very important in civilization [1]. They are wildly used in mineral exploration [2,3]. They are also utilized in soil tests [4], beside their applications in detecting trace elements in plants and organisms [5,6]. Recently spectrometers are used in medicine in diagnosis [7].

Spectrometers are devices that account for the concentration of elements in any sample [8]. They consist of detectors which detect electromagnetic waves by converting them to corresponding electrical pulses. Some detectors can also detect other energy forms and convert them to useful signals.

A frequency or wavelength splitter unit is important for the spectrometer to split the spectrum of the sample [9]. The spectrum of sample is displayed on the display unit screen as a wavelength (or frequency) versus the photons intensity. The wavelengths are related to elemental content of samples [9]. The photon intensity is related to the concentration of elements in the sample [10].

There are a wide variety of spectrometers that detect visible light photons emitted by atoms such as atomic absorption spectrometers. Some based on detecting x-ray emitted by atoms like are x-ray fluorescence spectrometer [11, 12, and 13]. Recently new simple techniques utilize electrical methods for mineral exploration [14, 15].

The behavior of atoms in a solid material can be explained by using quantum mechanics as well statistical Physics. This explanation is related to the fact. That solid consist of a large number of atoms and molecules. The

electrons and atoms of a solid can explained by using the laws of quantum mechanics. According to Maxwell distribution the density of photons proportional to the exited atoms or electrons density. [16, 17]

The atomic spectra are used in mineral exploration. It is also used in identification of the elemental content of solids, liquids, plants, tissues and bloods. [18, 19]

These elemental contents are useful in understanding the behavior of earth curst, plants, living organisms as well as environmental pollution.
These wide applications of atomic spectrometer show the importance of this technique. However, the spectrometers are expensive and needs complex procedures to analyze results [20 , 21]. Thus there is a need for simple spectral technique. One of the promising ones is the electrical method.

This electrical method was used by some researchers to find energy bands for semiconductors [8, 9].Unfortunately this method cannot identify minerals and conductors. Motivated by this new technique an experimental work was done to see how this electrical method can identify conductors by observing and determining the variation of conductivity with the frequency of current induced on it.

(1.2)Research problem

The spectrometers are very expensive. Therefore they are not widely spreaded in labs and fields. Several attempts were made to design spectrometers which are very complex and expensive.

(1.3) Literature Review

Many attempts were made for using simple techniquesfor mineral exploration.Identification of elements is very important in mineral exploration.

Most of spectrometers utilize electromagnetic spectrum to identify elements existing in samples like [Al, Cu, Au, Ag, Sn, Fe]. However some attempts were made to identify some materials by determining their energy gap, using simple electrical methods .Unfortunately such attempts can identify insulators and semiconductors but they cannot identify conductors or minerals [7]. This requires searching for simple alternative to do this.

In some works a direct inductive coupling between the transmitter and the receiver coil (induction balance, (IB) was used. In sensing heads based onthe transmitter-bucking configuration, IB is achieved by using two concentric transmitter coils with opposing exciter fields in order to create a central magnetic cavity for the receiver coil. This design has numerous advantages over other IB methods in terms of detection sensitivity, spatial resolution, sensor dimensions and suitability for model-based measurements. However, very careful design and precise sensing head geometry are required if a single excitation source is used for driving both transmitter coils. In this section we analyze the IB sensitivity to small perturbations of geometrical properties of coils. In this work a sensor design was proposed with dual current source and active induction balance scheme which overcomes the limitations of geometrybased. balancing and potentially provides more efficient compensation of soil effects.

Another methodology is based on quantum mechanics for assigning quantum conductivity when an AC field is applied across a variable gap between two plasmonic nanoparticles with an insulator sandwiched between them. The quantum tunneling effect is portrayed by a set of quantum conductivity coefficients describing the linear ac conductivity responding at the frequency of the applied field and nonlinear coefficients that modulate the field amplitude at the fundamental frequency and its harmonics. The quantum conductivity, determined with no fit parameters, has both frequency and gap

dependence that can be applied to determine the nonlinear quantum effects of strong applied electromagnetic fields even when the system is composed of dissimilar metal nanostructures. Our methodology compares well to results on quantum tunneling effects reported in the literature and it is simple to extend it to a number of systems with different metals and different insulators between them.

(1.4)Aim of the Work

This work aims to utilize physical laws of atomic spectra and interaction of electromagnetic waves with matter to design a simple spectrometer. This simple spectrometer is based on electric properties of matter.

(1.5) Materials and Methods

1-Agold detector which utilizes microwaves or radio waves to detect gold only is brought as a basic part of the spectrometer.

2-The characteristic electromagnetic frequencies emitted by minerals are determined.

3-The interaction of radiation with matter including reflection, refraction, transmission and absorption is also studied to determine how minerals respond to these interactions.

4-Asuitable detector based on these interactions is selected to replace gold detector.

5-The wavelengths are spitted by using suitable diffraction splitter or by using Fourier transform and suitable software.

6-The splitter unit is added to the gold detector.

7-Adisplay unit with interface are assembled and attached to the gold detector to display sample spectrum.

8-About 50 to 100 samples are prepared to determine the concentration of minerals within them.

9-These samples are analyzed by suitable standard spectrometer like X-ray fluorescence (XRF) or atomic absorption spectrometer (AAS).

10-The results of the designed spectrometers are compared with the standard results and the discrepancies are explained.

(1.6)Thesis lay out

This work has come into four chapters. Chapter two introducedfor theoretical background, then in chapter three literature reviews, and chapter four explains the experimental methods, the experimental results are discussion and conclusion remarks.

Chapter Two

Quantum Theory and Mineral Exploration

(2.1)Introduction

The simplest form of a metal detector consists of an oscillator producing an alternating current that passes through a coil producing an alternating magnetic field. If a piece of electrically conductive metal is close to the coil, eddy currents will be induced in the metal, and this produces a magnetic field of its own, If another coil is used to measure the magnetic field (acting as a magnetometer).the change in the magnetic field due to the metallic object can be detected.The first industrial metal detectors were developed in the 1960s and were used extensively for mining and other industrial applications. Uses include demining (the detection of land mines), the detection of weapons such as knives and guns (especially in airport security), geophysical prospecting, archaeology and treasure hunting. Metal detectors are also used to detect foreign bodies in food, and in the construction industry to detect steel reinforcing bars in concrete and pipes and wires buried in walls and floors [22, 23, and 25].

(2.2) Quantum Schrödinger Equation

The Schrödinger equation is the key equation of quantum mechanics [26]. This second order, partial differential equation determines the spatial shape and temporal evolvement of a wave function in a given potential and for given boundary conditions. The one-dimensional Schrödinger equation is used when the particle of interest is confined to one spatial dimension .To derive the one-dimensional [27, 28].

Schrödinger equation, we start with the total energy equation, i.e. the sum of kinetic and potential energy.

$$E = \frac{P^2}{2m} + V \qquad (2.2.1)$$

Multiplying both sides by Ψ

$$E\Psi = \frac{P^2}{2m}\Psi + V\Psi \quad (2.2.2)$$

The wave function of free particle is given by

$$\Psi = e^{i(kx-wt)} \quad (2.2.3)$$

But according to Planck theory

$$E = \hbar w$$

$$P = \hbar k$$

$$\Psi = Ae^{\frac{i}{\hbar}(Px-Et)} \quad (2.2.4)$$

Therefore

$$\frac{\partial \Psi}{\partial t} = -\frac{i}{\hbar}E\Psi \quad (2.2.5)$$

$$\frac{\hbar}{i}\frac{\partial \Psi}{\partial t} = E\Psi$$

$$\frac{\partial \Psi}{\partial x} = \frac{\hbar}{i}P\Psi$$

$$\frac{\hbar}{i}\frac{\partial \Psi}{\partial x} = P\Psi$$

$$\frac{\partial^2 \Psi}{\partial x^2} = \left(\frac{\hbar}{i}P\right)^2 \Psi = -P^2\hbar^2\Psi$$

$$-\frac{1}{\hbar^2}\frac{\partial^2\Psi}{\partial x^2} = P^2\Psi$$

In three dimension

$$\frac{\hbar}{i}\nabla\Psi = P\Psi$$

$$-\hbar^2\nabla^2\Psi = P^2\Psi \quad (2.2.6)$$

Sub equation (2.2.5) and (2.2.6) in equation (2.2.2) yields

$$\frac{i}{\hbar}\frac{\partial\Psi}{\partial t} = -\frac{\hbar^2}{2m}\nabla^2\Psi + V\Psi \quad (2.2.7)$$

This is the ordinary Schrödinger equation.

(2.3) Atomic Spectra and Element Identification

According to Quantum mechanics atoms have certain energy levels [29].

For Hydrogen atom the energy of electron is given by

$$E_n = -\frac{me^4z^2}{8\varepsilon_0 h^2 n^2} \quad (2.3.1)$$

Where*n*= 1, 2, 3…. and is called the Principal Quantum Number.

Characterizing the energy level electrons exists in certain when

$$E_m - E_n = hf \quad (2.3.2)$$

(2.3.1) Atomic Absorption Spectrometry (AAS)

The absorption of energy by atoms follows well known physical laws which provide us with a basis for quantitative analytical chemistry. The radiant energy or photons, absorbed by atoms are generally in the form of very narrow

lines of characteristic wavelength originating from the visible or ultraviolet spectrum [30].

During the absorption process the outer valence electrons of the atoms are promoted to a higher orbital and the atom is electronically excited. There is a relationship and equilibrium between the populations of excited and unexcited atoms involving photons, and between atomic absorption and atomic emission spectroscopy [31, 32, and 33].

A photon behaves in a similar manner to an alternating electric field and interacts with the negatively charged electrons in an atom. Under certain conditions a photon can be absorbed by an atom. The energy levels in an atom are quantized, that is they have certain well defined energies. As a consequence of this, the photon energy, hf, must be exactly equal to the energy gap between a filled energy level $E_0$the ground state, and an unoccupied energy level $E_1$the first excited state [34, 35].

Atomic Absorption Spectrometry (AAS) is a technique for measuring quantities of chemical elements present in environmental samples by measuring the absorbed radiation by the chemical element of interest. This is done byreading the spectra produced when the sample is excited by radiation. The atoms absorb ultraviolet or visible light and make transitions to higher energy levels. Atomic absorption methods measure the amount of energy in the form of photons of light that are absorbed by the sample. A detector measures the wavelengths of light transmitted by the sample, and compares them to the wavelengths which originally passed through the sample. A signal processor then integrates the changes in wavelength absorbed, which appear in the readout as peaks of energy absorption at discrete wavelengths. The energy required for an electron to leave an atom is known as ionization energy and is specific to each chemical element. When an electron moves from one energy level to another within the atom,

A photon is emitted with energy E. Atoms of an element emit a characteristic spectral line. Every atom has its own distinct pattern of wavelengths at which it will absorb energy, due to the unique configuration of electrons in its outer shell.

This enables the qualitative analysis of a sample. The concentration is calculated based on the Beer-Lambert law. Absorbance is directly proportional to the concentration of the atoms of the sample. The concentration is usually determined from a calibration curve, obtained using standards of known concentration. However, applying the Beer-Lambert law directly in AAS is difficult due to: variations in atomization efficiency from the sample matrix, non-uniformity of concentration and path length of analyze atoms (in graphite furnace AA) [36, 37].

The chemical methods used are based on matter interactions, i.e. chemical reactions. For a long period of time these methods were essentially empirical, involving, in most cases, great experimental skills. In analytical chemistry, AAS is a technique used mostly for determining the concentration of a particular metal element within a sample. AAS can be used to analyze the concentration of over 62 different metals in a solution [38].

Although AAS dates to the nineteenth century, the modern form of this technique was largely developed during the 1950s by Alan Walsh and a team of Australian chemists working at the CSIRO (Commonwealth Science and Industry Research Organization) Division of Chemical Physics in Melbourne, Australia. Typically, the technique makes use of a flame to atomize the sample, but other atomizers,such as a graphite furnace, are also used.

Three steps are involved in turning a liquid sample into an atomic gas:

1. Desolvation – the liquid solvent is evaporated, and the dry sample remains.
2. Vaporization – the solid sample vaporizes to a gas.

3. Volatilization – the compounds that compose the sample are broken into free atoms [39].

To measure how much of a given element is present in a sample, one must first establish a basis for comparison using known quantities of that element to produce a calibration curve.

To generate this curve, a specific wavelength is selected, and the detector is set to measure only the energy transmitted at that wavelength. As the concentration of the target atom in the sample increases, the absorption will also increase proportionally. A series of samples containing known concentrations of the compound of interest are analyzed, and the corresponding absorbance, which is the inverse percentage of light transmitted, is recorded [40].

The measured absorption at each concentration is then plotted, so that a straight line can then be drawn between the resulting points. From this line, the concentration of the substance under investigation is extrapolated from the substance's absorbance. The use of special light sources and the selection of specific wavelengths allow for the quantitative determination of individual components in a multielement mixture [41].

(2.3.2) X-ray fluorescence

X-ray fluorescence (XRF) is the emission of characteristic "secondary" (or fluorescent) X-rays from a material that has been excited by bombarding with high-energy X-rays or gamma rays. The phenomenon is widely used for elemental analysis and chemical analysis, particularly in the investigation of metals, glass, ceramics and building materials, and for research in geochemistry, forensic science and archaeology.[70]

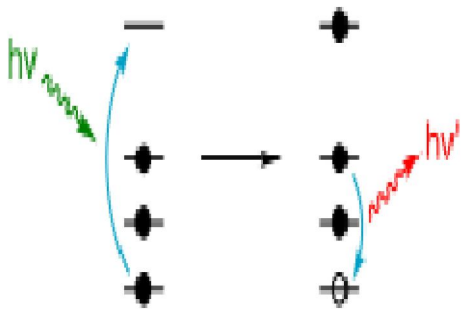

Fig (2.1): Physics of X-ray fluorescence in a schematic representation. [42]

When materials are exposed to short-wavelength X-rays or to gamma rays, ionization of their component atoms may take place. Ionization consists of the ejection of one or more electrons from the atom, and may occur if the atom is exposed to radiation with energy greater than its ionization potential. X-rays and gamma rays can be energetic enough to expel tightly held electrons from the inner orbitals of the atom. The removal of an electron in this way makes the electronic structure of the atom unstable, and electrons in higher orbital's "fall" into the lower orbital to fill the hole left behind. In falling, energy is released in the form of a photon, the energy of which is equal to the energy difference of the two orbitals involved. Thus, the material emits radiation, which has energy characteristic of the atoms present. The term fluorescence is applied to phenomena in which the absorption of radiation of a specific energy results in the re-emission of radiation of a different energy (generally lower) [42].

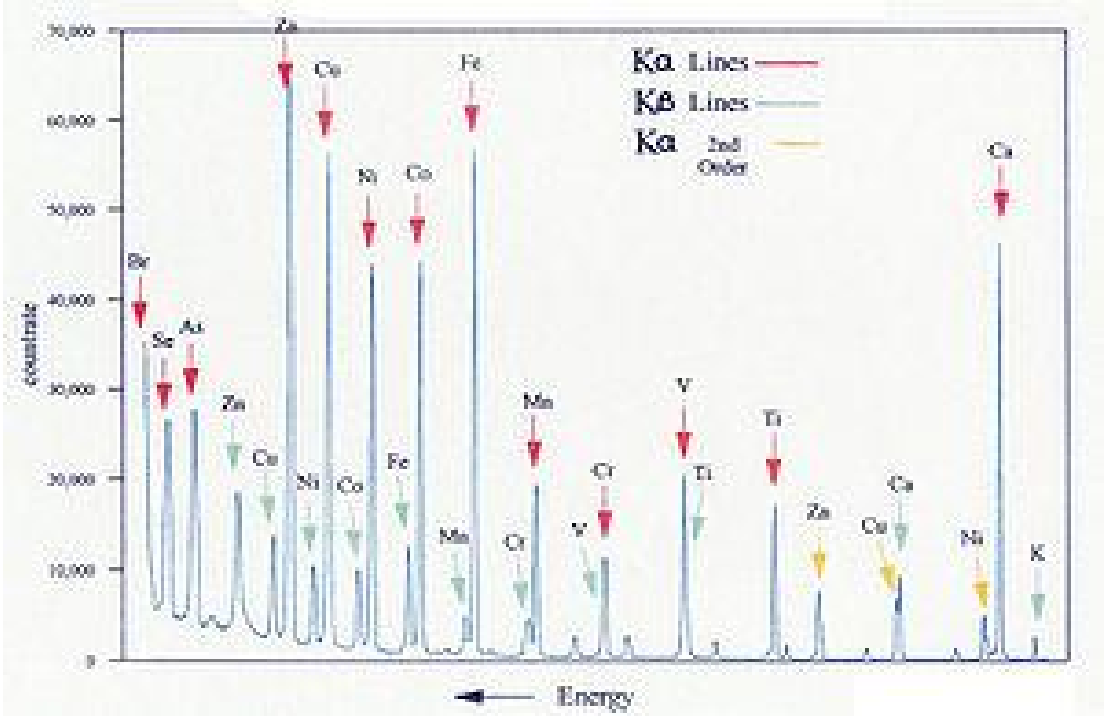

Fig (2.2): Typical wavelength dispersive XRF spectrum. [44]

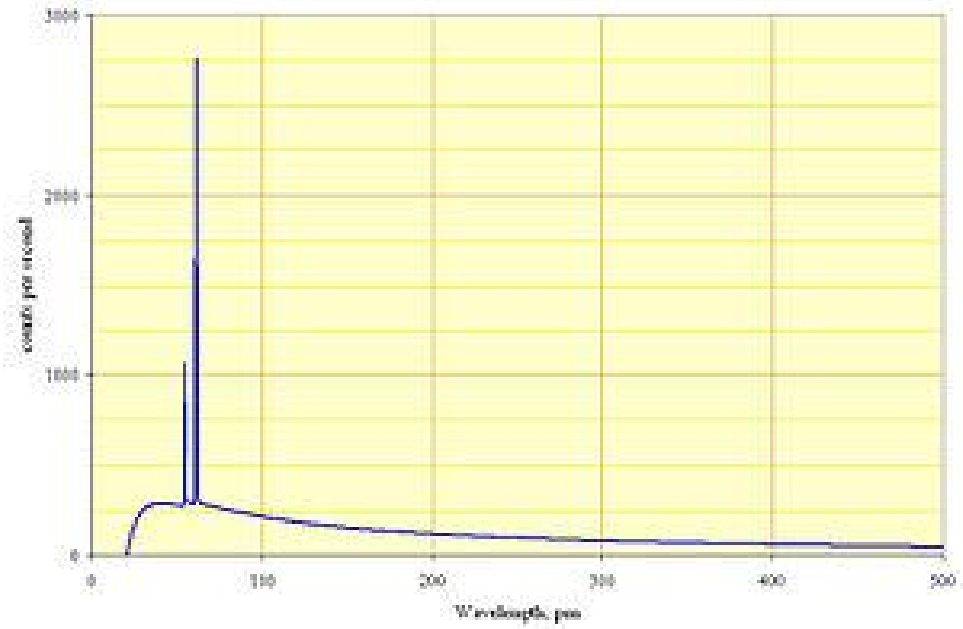

Fig (2.3): Spectrum of a rhodium target tube operated at 60 kV, showing continuous spectrum and K lines. [44]

Each element has electronic orbitals of characteristic energy. Following removal of an inner electron by an energetic photon provided by a primary radiation source, an electron from an outer shell drops into its place. There are a limited number of ways in which this can happen, as shown in Figure 1. The main transitions are given names: an L→K transition is traditionally called K_α, an M→K transition is called K_β, an M→L transition is called L_α, and so on. Each of these transitions yields a fluorescent photon with a characteristic energy equal to the difference in energy of the initial and final orbital [44]. The wavelength of this fluorescent radiation can be calculated from Planck's Law:

$$\lambda = h \cdot c / E$$

The fluorescent radiation can be analyzed either by sorting the energies of the photons (energy-dispersive analysis) or by separating the wavelengths

of the radiation (wavelength-dispersive analysis). Once sorted, the intensity of each characteristic radiation is directly related to the amount of each element in the material. This is the basis of a powerful technique in analytical chemistry. Figure 2 shows the typical form of the sharp fluorescent spectral lines obtained in the energy-dispersive method (see Moseley's law).In energy dispersive analysis, dispersion and detection are a single operation, as already mentioned above. Proportional counters or various types of solid-state detectors (PIN diode, Si(Li), Ge(Li), Silicon Drift Detector SDD) are used. They all share the same detection principle: An incoming X-ray photon ionizes a large number of detector atoms with the amount of charge produced being proportional to the energy of the incoming photon. The charge is then collected and the process repeats itself for the next photon. Detector speed is obviously critical; as all charge carriers measured have to come from the same photon to measure the photon energy correctly (peak length discrimination is used to eliminate events that seem to have been produced by two X-ray photons arriving almost simultaneously). The spectrum is then built up by dividing the energy spectrum into discrete bins and counting the number of pulses registered within each energy bin. EDXRF detector types vary in resolution, speed and the means of cooling (a low number of free charge carriers is critical in the solid state detectors): proportional counters with resolutions of several hundred eV cover the low end of the performance spectrum, followed by PIN diode detectors, while the Si(Li), Ge(Li) and Silicon Drift Detectors (SDD) occupy the high end of the performance scale. In wavelength dispersive analysis, the single-wavelength radiation produced by the monochromatic is passed into a photomultiplier, a detector similar to a Geiger counter, which counts individual photons as they pass through. The counter is a chamber containing a gas that is ionized by X-ray photons. A central electrode is charged at (typically) +1700 V with respect to the

conducting chamber walls, and each photon triggers a pulse-like cascade of current across this field. The signal is amplified and transformed into an accumulating digital count. These counts are then processed to obtain analytical data [43,45].

The fluorescence process is inefficient, and the secondary radiation is much weaker than the primary beam. Furthermore, the secondary radiation from lighter elements is of relatively low energy (long wavelength) and has low penetrating power, and is severely attenuated if the beam passes through air for any distance. Because of this, for high-performance analysis, the path from tube to sample to detector is maintained under vacuum (around 10 Pa residual pressures). This means in practice that most of the working parts of the instrument have to be located in a large vacuum chamber. In energy dispersive spectrometers (EDX or EDS), the detector allows the determination of the energy of the photon when it is detected. Detectors historically have been based on silicon semiconductors, in the form of lithium-drifted silicon crystals, or high-purity silicon wafers. These consist essentially of a 3–5 mm thick silicon junction type P-I-N diode (same as PIN diode) with a bias of −1000 V across it. The lithium-drifted centre part forms the non-conducting i-layer, where Li compensates the residual acceptors which would otherwise make the layer p-type. When an X-ray photon passes through, it causes a swarm of electron-hole pairs to form, and this causes a voltage pulse. To obtain sufficiently low conductivity, the detector must be maintained at low temperature, and liquid-nitrogen must be used for the best resolution. With some loss of resolution, the much more convenient Peltier cooling can be employed.Morerecently, high-purity silicon wafers with low conductivity have become routinely available. Cooled by the Peltier effect, this provides a cheap and convenient detector, although the liquid nitrogen cooled Si(Li)

detector still has the best resolution (i.e. ability to distinguish different photon energies)[46].

The pulses generated by the detector are processed by pulse-shaping amplifiers.In wavelength dispersive spectrometers (WDX or WDS), the photons are separated by diffraction on a single crystal before being detected. Although wavelength dispersive spectrometers are occasionally used to scan a wide range of wavelengths, producing a spectrum plot as in EDS, they are usually set up to make measurements only at the wavelength of the emission lines of the elements of interest. This is achieved in two different ways:

"Simultaneous" spectrometers have a number of "channels" dedicated to analysis of a single element, each consisting of a fixed-geometry crystal monochromator, a detector, and processing electronics. This allows a number of elements to be measured simultaneously, and in the case of high-powered instruments, complete high-precision analyses can be obtained in under 30 s. Another advantage of this arrangement is that the fixed-geometry monochromators have no continuously moving parts, and so are very reliable.

"Sequential" spectrometers have a single variable-geometry monochromator (but usually with an arrangement for selecting from a choice of crystals), a single detector assembly (but usually with more than one detector arranged in tandem), and a single electronic pack. The instrument is programmed to move through a sequence of wavelengths, in each case selecting the appropriate X-ray tube power, the appropriate crystal, and the appropriate detector arrangement. The length of the measurement program is essentially unlimited, so this arrangement is very flexible. Because there is only one monochromator, the tube-sample-crystal distances can be kept very short, resulting in minimal loss of detected intensity. The obvious disadvantage is relatively long analysis time, particularly when many elements

are being analyzed [47].The spectral lines used for chemical analysis are selected on the basis of intensity, accessibility by the instrument, and lack of line overlaps. Typical lines used, and their wavelengths, are as follows:

Element	Line	wavelength (nm)	Element	line	wavelength (nm)	Element	line	wavelength (nm)
Li	Kα	22.8	Ni	Kα1	0.1658	I	Lα1	0.3149
Be	Kα	11.4	Cu	Kα1	0.1541	Xe	Lα1	0.3016
B	Kα	6.76	Zn	Kα1	0.1435	Cs	Lα1	0.2892
C	Kα	4.47	Ga	Kα1	0.1340	Ba	Lα1	0.2776
N	Kα	3.16	Ge	Kα1	0.1254	La	Lα1	0.2666
O	Kα	2.362	As	Kα1	0.1176	Ce	Lα1	0.2562
F	Kα1,2	1.832	Se	Kα1	0.1105	Pr	Lα1	0.2463
Ne	Kα1,2	1.461	Br	Kα1	0.1040	Nd	Lα1	0.2370
Na	Kα1,2	1.191	Kr	Kα1	0.09801	Pm	Lα1	0.2282
Mg	Kα1,2	0.989	Rb	Kα1	0.09256	Sm	Lα1	0.2200
Al	Kα1,2	0.834	Sr	Kα1	0.08753	Eu	Lα1	0.2121
Si	Kα1,2	0.7126	Y	Kα1	0.08288	Gd	Lα1	0.2047
P	Kα1,2	0.6158	Zr	Kα1	0.07859	Tb	Lα1	0.1977
S	Kα1,2	0.5373	Nb	Kα1	0.07462	Dy	Lα1	0.1909
Cl	Kα1,2	0.4729	Mo	Kα1	0.07094	Ho	Lα1	0.1845
Ar	Kα1,2	0.4193	Tc	Kα1	0.06751	Er	Lα1	0.1784
K	Kα1,2	0.3742	Ru	Kα1	0.06433	Tm	Lα1	0.1727
Ca	Kα1,2	0.3359	Rh	Kα1	0.06136	Yb	Lα1	0.1672
Sc	Kα1,2	0.3032	Pd	Kα1	0.05859	Lu	Lα1	0.1620
Ti	Kα1,2	0.2749	Ag	Kα1	0.05599	Hf	Lα1	0.1570
V	Kα1	0.2504	Cd	Kα1	0.05357	Ta	Lα1	0.1522
Cr	Kα1	0.2290	In	Lα1	0.3772	W	Lα1	0.1476
Mn	Kα1	0.2102	Sn	Lα1	0.3600	Re	Lα1	0.1433
Fe	Kα1	0.1936	Sb	Lα1	0.3439	Os	Lα1	0.1391
Co	Kα1	0.1789	Te	Lα1	0.3289	Ir	Lα1	0.1351

Other lines are often used, depending on the type of sample and equipment available.

Detectors used for wavelength dispersive spectrometry need to have high pulse processing speeds in order to cope with the very high photon count rates that can be obtained. In addition, they need sufficient energy resolution to allow filtering-out of background noise and spurious photons from the primary beam or from crystal fluorescence [48].

There are four common types of detector:

_ gas flow proportional counters.

_ sealed gas detectors.

_scintillation counters.

_semiconductor detectors.

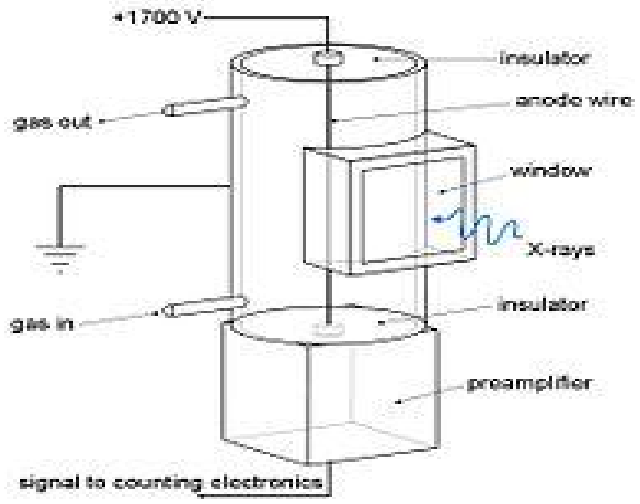

Fig (2.4): Arrangement of gas flow proportional counter. [48]

Gas flow proportional counters are used mainly for detection of longer wavelengths. Gas flows through it continuously. Where there are multiple detectors, the gas is passed through them in series, then led to waste. The gas is usually 90% argon, 10% methane ("P10"), although the argon may be

replaced with neon or helium where very long wavelengths (over 5 nm) are to be detected. The argon is ionized by incoming X-ray photons, and the electric field multiplies this charge into a measurable pulse. The methane suppresses the formation of fluorescent photons caused by recombination of the argon ions with stray electrons. The anode wire is typically tungsten or nichrome of 20–60 μmdiameter. Since the pulse strength obtained is essentially proportional to the ratio of the detector chamber diameter to the wire diameter, a fine wire is needed, but it must also be strong enough to be maintained under tension so that it remains precisely straight and concentric with the detector.

Scintillation counters consist of a scintillating crystal (typically of sodium iodide doped with thallium) attached to a photomultiplier. The crystal produces a group of scintillations for each photon absorbed, the number being proportional to the photon energy. This translates into a pulse from the photomultiplier of voltage proportional to the photon energy. Scintillation counters are often connected in series with a gas flow proportional counter: the latter is provided with an outlet window opposite the inlet, to which the scintillation counter is attached [49].

Semiconductor detectors can be used in theory, and their applications are increasing as their technology improves, but historically their use for WDX has been restricted by their slow response [50].

A glass "bead" specimen for XRF analysis being cast at around 1100 °C in a Herzog automated fusion machine in a cement plant quality control laboratory. 1 (top): fusing, 2: preheating the mould, 3: pouring the melt, 4: cooling the "bead"

At first sight, the translation of X-ray photon count-rates into elemental concentrations would appear to be straightforward: WDX separates the X-ray

lines efficiently, and the rate of generation of secondary photons is proportional to the element concentration. However, the number of photons leaving *the* sample is also affected by the physical properties of the sample: so-called "matrix effects"[51]. These fall broadly into three categories:

- X-ray absorption.

-X-ray enhancement.

-Sample macroscopic effects.

All elements *absorb* X-rays to some extent. Each element has a characteristic absorption spectrum which consists of a "saw-tooth" succession of fringes, each step-change of which has wavelength close to an emission line of the element. Absorption attenuates the secondary X-rays leaving the sample. For example, the mass absorption coefficient of silicon at the wavelength of the aluminum Kα line is 50m²/kg, whereas that of iron is 377m²/kg. This means that a given concentration of aluminium in a matrix of iron gives only one seventh of the count rate compared with the same concentration of aluminium in a silicon matrix. Fortunately, mass absorption coefficients are well known and can be calculated. However, to calculate the absorption for a multi-element sample, the composition must be known. For analysis of an unknown sample, an iterative procedure is therefore used. It will be noted that, to derive the mass absorption accurately, data for the concentration of elements not measured by XRF may be needed, and various strategies are employed to estimate these. As an example, in cement analysis, the concentration of oxygen (which is not measured) is calculated by assuming that all other elements are present as standard oxides [52,53].

Enhancement occurs where the secondary X-rays emitted by a heavier element are sufficiently energetic to stimulate additional secondary emission from a lighter element. This phenomenon can also be modelled, and corrections can be made provided that the full matrix composition can be deduced [54].

Sample macroscopic effects consist of effects of in homogeneities of the sample, and unrepresentative conditions at its surface. Samples are ideally homogeneous and isotropic, but they often deviate from this ideal. Mixtures of multiple crystalline components in mineral powders can result in absorption effects that deviate from those calculable from theory. When a powder is pressed into a tablet, the finer minerals concentrate at the surface. Spherical grains tend to migrate to the surface more than do angular grains. In machined metals, the softer components of an alloy tend to smear across the surface. Considerable care and ingenuity are required to minimize these effects. Because they are artifacts of the method of sample preparation, these effects cannot be compensated by theoretical corrections, and must be "calibrated in". This means that the calibration materials and the unknowns must be compositionally and mechanically similar, and a given calibration is applicable only to a limited range of materials. Glasses most closely approach the ideal of homogeneity and isotropy, and for accurate work, minerals are usually prepared by dissolving them in a borate glass, and casting them into a flat disc or "bead". Prepared in this form, a virtually universal calibration is applicable [55].

Further corrections that are often employed include background correction and line overlap correction. The background signal in an XRF spectrum derives primarily from scattering of primary beam photons by the sample surface. Scattering varies with the sample mass absorption, being

greatest when mean atomic number is low. When measuring trace amounts of an element, or when measuring on a variable light matrix, background correction becomes necessary. This is really only feasible on a sequential spectrometer. Line overlap is a common problem, bearing in mind that the spectrum of a complex mineral can contain several hundred measurable lines. Sometimes it can be overcome by measuring a less-intense, but overlap-free line, but in certain instances a correction is inevitable. For instance, the Kα is the only usable line for measuring sodium, and it overlaps the zinc Lβ (L_2-M_4) line. Thus zinc, if present, must be analyzed in order to properly correct the sodium value [56].

The concentration of $C_i$the element i is proportional to the Intensity$I_i$of the spectrum peak, i.e

$$C_i = a_i I_i + b_i$$

Where a_i and b_i are constants.

(2.4) Current Density and Conductivity

In this section, we study the effects of moving charges due to an external electric field. The measure of the movement of charge is current and is defined as:

There are three types of currents that we are interested in:

Conductor current: The current that flows through conductors, semiconductors and insulators.

Electrolytic current: The current that results from ionized solutions such as batteries.

Convection current: The current flow through vacuum or gaseous mediums.

The current density may be defined as the volume charge density of a conductor multiplied by the charge [57].

The Electric Current Density is denoted by the vector symbol (**J**). Electric current is measured in Amps (which is equal to charge per second [C/s]). The current density (which is a volume current density) is measured in Amps per meter squared [A/m^2], because the current flows in a direction, and the area is measured normal/perpendicularly/orthogonally to that.

The total electric current (**I**) can be related to the current density (**J**) by summing up (or integrating) the current density over the area.

This page is about the electric current density in electromagnetism. For the probability current density in quantum mechanics [60].

In electromagnetism, current density is the electric current per unit area of cross section. It is defined as a vector whose magnitude is the electric current per cross-sectional area at a given point in space (i.e. it is a vector field). In SI units, the electric current density is measured in amperes per square meter [66].

Electric current density J is simply the current I (SI unit: A) per unit area$A$ (SI unit: m^2). Its magnitude.

For current density as a vector **J**, the surface integral over a surface$S$, followed by an integral over the time duration t_1 to t_2, gives the total amount of charge flowing through the surface in that time ($t_2 - t_1$).

The area required to calculate the flux is real or imaginary, flat or curved, either as a cross-sectional area or a surface. For example, for charge carriers passing through an electrical conductor, the area is the cross-section of the conductor, at the section considered [58].

The vector area is a combination of the magnitude of the area through which the mass passes through, A, and a unit vector normal to the area.

If the current density **J** passes through the area at an angle θ to the area normal .

This is, the component of current density passing through the surface (i.e. normal to it) is Jcos θ, while the component of current density passing tangential to the area is *J* sin θ, but there is no current density actually passing through the area in the tangential direction. The only component of current density passing normal to the area is the cosine component [59].
Current density is important to the design of electrical and electronic systems.

Circuit performance depends strongly upon the designed current level, and the current density then is determined by the dimensions of the conducting elements. For example, as integrated circuits are reduced in size, despite the lower current demanded by smaller devices, there is trend toward higher current densities to achieve higher device numbers in ever smaller chip areas. See Moore's law.

At high frequencies, current density can increase because the conducting region in a wire becomes confined near its surface, the so-called skin effect.

High current densities have undesirable consequences. Most electrical conductors have a finite, positive resistance, making them dissipate power in the form of heat. The current density must be kept sufficiently low to prevent the conductor from melting or burning up, the insulating material failing, or the desired electrical properties changing. At high current densities the material forming the interconnections actually moves, a phenomenon called electro migration. In superconductors excessive current density may generate a strong enough magnetic field to cause spontaneous loss of the superconductive property [61].

The analysis and observation of current density also is used to probe the physics underlying the nature of solids, including not only metals, but also semiconductors and insulators. An elaborate theoretical formalism has developed to explain many fundamental observations [63].

The current density is an important parameter in Ampère's circuital law (one of Maxwell's equations), which relates current density to magnetic field.

In special relativity theory, charge and current are combined into a 4-vector.

Charge carriers which are free to move constitute a free current density, which are given by expressions such as those in this section.

Electric current is a coarse, average quantity that tells what is happening in an entire wire. At position r at time t, the *distribution* of charge flowing is described by the current density $\mathbf{J}(\mathbf{r}, t)$ is the current density vector, $\mathbf{v}_d(\mathbf{r}, t)$ is the particles' average drift velocity (SI unit: $\mathrm{m \cdot s^{-1}}$), and is the charge density (SI unit: coulombs per cubic meter), in which $n(\mathbf{r}, t)$ is the number of particles per unit volume ("number density") (SI unit: $\mathrm{m^{-3}}$), q is the charge of the individual particles with density n (SI unit: coulombs).

A common approximation to the current density assumes the current simply is proportional to the electric field, as expressed by:

$$j = \sigma \ E \ = nev$$

Where**E** is the electric field and σ is the electrical conductivity.

Conductivity σ is the reciprocal (inverse) of electrical resistivity and has the SI units of Siemens per meter ($\mathrm{S\ m^{-1}}$), and **E** has the SI units of newtons per coulomb ($\mathrm{N\ C^{-1}}$) or, equivalently, volts per meter ($\mathrm{V\ m^{-1}}$).

Indicating the lag in response by the time dependence of σ, and the non-local nature of response to the field by the spatial dependence of σ, both calculated in principle from an underlying microscopic analysis, for example, in the case of small enough fields, the linear response function for the conductive behavior in the material. See, for example, Giuliani or Rammer. The integral extends over the entire past history up to the present time [61].

The above conductivity and its associated current density reflect the fundamental mechanisms underlying charge transport in the medium, both in time and over distance.

In many materials, for example, in crystalline materials, the conductivity is a tensor, and the current is not necessarily in the same direction as the applied field. Aside from the material properties themselves, the application of magnetic fields can alter conductive behavior.

Currents arise in materials when there is a non-uniform distribution of charge.

In dielectric materials, there is a current density corresponding to the net movement of electric dipole moments per unit volume, i.e. the polarization**P**.

Similarly with magnetic materials, circulations of the magnetic dipole moments per unit volume, i.e. the magnetization**M** lead to volume magnetization currents.Together, these terms form adds up to the bound current density in the material (resultant current due to movements of electric and magnetic dipole moments per unit volume).The total current is simply the sum of the free and bound currents.

There is also a displacement current corresponding to the time-varying electric displacement field**D**.

Which is an important term in Ampere's circuital law, one of Maxwell's equations, since absence of this term would not predict electromagnetic waves to propagate, or the time evolution of electric fields in general[68].

Since charge is conserved, current density must satisfy a continuity equation. Here is a derivation from first principles.

The net flow out of some volume V (which can have an arbitrary shape but fixed for the calculation) must equal the net change in charge held inside the volume.

The surface integral on the left expresses the current outflow from the volume, and the negatively signed volume integral on the right expresses the decrease in the total charge inside the volume.

In electrical wiring, the maximum current density can vary from $4\text{A}\cdot\text{mm}^{-2}$ for a wire with no air circulation around it, to $6\text{A}\cdot\text{mm}^{-2}$ for a wire in free air. Regulations for building wiring list the maximum allowed current of each size of cable in differing conditions. For compact designs, such as windings of SMPS transformers, the value might be as low as $2\ \text{A}\cdot\text{mm}^{-2}$. If the wire is carrying high frequency currents, the skin effect may affect the distribution of the current across the section by concentrating the current on the surface of the conductor. In transformers designed for high frequencies, loss is reduced if Litz wire is used for the windings. This is made of multiple isolated wires in parallel with a diameter twice the skin depth. The isolated strands are twisted together to increase the total skin area and to reduce the resistance due to skin effects.

For the top and bottom layers of printed circuit boards, the maximum current density can be as high as $35\ \text{A}\cdot\text{mm}^{-2}$ with a copper thickness of

35 μm. Inner layers cannot dissipate as much heat as outer layers; designers of circuit boards avoid putting high-current traces on inner layers[63].

In semiconductors, the maximum current density is given by the manufacturer. A common average is 1 mA·μm^{-2} at 25 °C for 180 nm technology. Above the maximum current density, apart from the joule effect, some other effects like electro migration appear in the micrometer scale.

In biological organisms, ion channels regulate the flow of ions (for example, sodium, calcium, potassium) across the membrane in all cells. Current density is measured in pA·pF^{-1} (picoamperes per picofarad), that is, current divided by capacitance, a de facto measure of membrane area.

In gas discharge lamps, such as flash lamps, current density plays an important role in the output spectrum produced. Low current densities produce spectral lineemission and tend to favor longer wavelengths. High current densities produce continuum emission and tend to favor shorter wavelengths. Low current densities for flash lamps are generally around 1000 A·cm^{-2}. High current densities can be more than 4000 A·cm^{-2}[62].

The Probability Current Density is given by:

$$\frac{\partial}{\partial t}\int p d^3r = \int \frac{\partial |\Psi|^2}{\partial t} d^3r = \int \frac{\partial}{\partial t}\Psi^*\Psi d^3r$$

$$= \int \left[\Psi^* \frac{\partial \Psi}{\partial t} + \frac{\partial \Psi^*}{\partial t}\Psi\right] d^3r \qquad (2.4.1)$$

But from Schrödinger equation:

$$\frac{i\partial\Psi}{\partial t} = \frac{-\hbar^2}{2m}\nabla^2\Psi + U\Psi \quad , \quad \frac{-i\hbar\partial\Psi^*}{\partial t} = \frac{-\hbar^2}{2m}\nabla^2\Psi^* + U\Psi^*$$

$$\frac{\partial\Psi}{\partial t} = \frac{-i\hbar^2}{2m}\nabla^2\Psi - iU\Psi \quad , \quad \frac{\hbar\partial\Psi^*}{\partial t} = \frac{-i\hbar^2}{2m}\nabla^2\Psi^* + iU\Psi^* \quad (2.4.2)$$

Thus:

$$\frac{\partial}{\partial t}\int p d^3r = \frac{i\hbar}{2m}\int \Psi^*\nabla^2\Psi - \Psi\nabla^2\Psi^* d^3r$$

$$=\frac{i\hbar}{2m}\int \nabla.[\Psi^*\nabla\Psi - (\nabla\Psi^*)\Psi]d^3r$$

$$=\frac{i\hbar}{2m}\int \nabla.S\, d^3r=\frac{i\hbar}{2m}\int \nabla.[\Psi^*\nabla\Psi - (\nabla\Psi^*)\Psi]dA \qquad (2.4.3)$$

But the continuity equation reads:

$$\frac{\partial\rho}{\partial t} + \nabla.J = 0 \qquad (2.4.4)$$

In view of (2.4.3):

$$\frac{\partial\rho}{\partial t} + \nabla.S = 0 \qquad (2.4.5)$$

Thus S represents the Intensity of particles, i .e the flux of particles

Crossing unit area per unit time, where:

$$S=\frac{i\hbar}{2m}[\Psi^*\nabla\Psi - \Psi(\nabla\Psi^*)] \qquad (2.4.6)$$

It is well known that the momentum operator is hermition.

Hence:

$$\int \hat{P}\overline{\Psi}\,\Psi d^3r=\int \overline{\Psi}\hat{P}\,\Psi d^3r$$

$$-\frac{\hbar}{i}\int \nabla\Psi^*\,\Psi d^3r = -\frac{\hbar}{i}\int \Psi^*\,\nabla\Psi d^3r$$

Hence:

$$\Psi\nabla\Psi^* = -\Psi^*\nabla\Psi$$

Therefore:

$$S = \frac{i\hbar}{2m}[2\Psi^*\nabla\Psi]$$

$$S = \frac{i\hbar}{m}\Psi^*\nabla\Psi \qquad (2.4.7)$$

Generally S =Real$[\frac{i\hbar}{m}\Psi^*\nabla\Psi]$

Electric current density is given by

$$J = eRe[\Psi^*\frac{h}{i}\nabla\Psi] \quad (2.4.8)$$

(2.4.1) Electric Conductivity

The question has been asked how loss, conductivity, and dielectric constant are interrelated. Answering this question requires a fairly extensive review of basic electromagnetic [66].

First, assume that one has a piece of arbitrary material. This material is made of atoms, molecules, or ions. Within this material exist electrons, either bound to individual atoms or free to move about. An electric field is applied across the object. The electrons will naturally want to move because of the electric field. The conduction electric current density (a measure of the flow of electrons) varies directly with the strength of the electric field [64]. Thus

$$J_c = \sigma_s \ E \ = nev \qquad \textbf{(2.4.1.1)}$$

Where σ_s is a constant of proportionality, and it is called "conductivity." The conductivity provides a measure of how fast an electron can flow through a material. It is defined as

$$\sigma_s \ = -q \ \mu_e \textbf{(2.4.1.2)}$$

Where q is the charge and μ_e is the electric mobility (not the permeability) of the medium.

Likewise, the electric flux density varies linearly with the application of the electric field so that

$$D = \varepsilon \bar{E} \textbf{(2.4.1.3)}$$

Here, ε is the constant of proportionality, and it is called "permittivity."

The time-harmonic version of Maxwell's equations states that

$$\nabla \times H = \bar{J} + j\omega \bar{D} \textbf{(2.4.1.4)}$$

J is the electric current density, and it has two parts. The first part is the impressed electric current density, $\overline{J_\iota}$ (that is, $\overline{J_\iota}$ is an excitation to the system by an outside source), and the second part is the aforementioned conduction electric

current density, $\overline{J_c}$, caused by the application of an external electric field. Thus, we have

$$\nabla \times H = \overline{J_\iota} + \overline{J_c} + j\omega \overline{D} \textbf{(2.4.1.5)}$$

$$\nabla \times H = \overline{J_\iota} + \sigma_s \overline{E} + j\omega \overline{D} \textbf{(2.4.1.6)}$$

In most materials there exists at least one of three types of electric dipoles. Any kind of dipole exhibits a polarity; that is, one side of the dipole can be described as being negatively charged, and the other side can be described as being positively charged. The three types of dipoles are as follows.

1. Molecules arranged in such a way as to exhibit an imbalance of charge. For instance, water is bound in such a way that the two negative hydrogen atoms are on one side of the molecule, and a positive oxygen atom is on the other side. Hence, water has a net electric polarity [65].

2. Ions have inherently oppositely charged parts. For instance, table salt, NaCl, has a positive sodium atom (Na^+) and a negative chlorine atom (Cl^-).

3. Most atoms have a cloud of electrons surrounding the nucleus. Since the mass of an electron is much less than the mass of the nucleus, the application

of an electric field causes the electrons to react and move much more quickly than the nucleus can react. The result is that the electron cloud shifts its position and is no longer centered about the nucleus. Hence, the atom ends with the positively charged nucleus on one side and the negatively charged electron cloud on the other side [66].

When an external electric field is applied, the dipoles align with the field. This action causes a term to be added to the electric flux density that has the same vector direction as the applied field. This relationship can be mathematically described as

$$\overline{\mathrm{D}} = \varepsilon_0 \overline{E} + \varepsilon_0 x_e \overline{E} \quad \textbf{(2.4.1.7)}$$

The term x_e is known as the electric susceptibility and serves as a proportionality constant between the electric field and the portion of the electric flux density caused by the presence of the dielectric. One can rewrite the equation as

$$\overline{\mathrm{D}} = \varepsilon_0 (1 + x_e) \overline{E} \quad \textbf{(2.4.1.8)}$$

or

$$\overline{\mathrm{D}} = \varepsilon_0 \varepsilon_r \overline{E} \quad \textbf{(2.4.1.9)}$$

Whereε_r is known as the relative permittivity of the medium.

ε_r is in general a complex quantity. To understand why, consider an alternating electric field applied to a dipole. When the field first strikes the dipole, the dipole rotates to align itself with the field. As time passes, the electric field reverses its direction and the dipole must rotate again to remain aligned with the correct polarity. As it rotates, energy is lost through the generation of heat (friction) as well as the acceleration and deceleration of the rotational motion of the dipole. The degree to which the dipole is out of phase with the incident electric field and the losses that ensue determine how large the imaginary part of the permittivity is as a function of material and frequency. The larger the imaginary part, the more energy is being dissipated

through motion, and the less energy is available to propagate past the dipole. Thus, the imaginary part of the relative permittivity directly relates to loss in the system.

To represent the real and imaginary parts of the absolute permittivity, the following convention is used [67].

In this last step, we have defined an effective conductivity:

$$\sigma_e = \sigma_s + \omega\ddot{\varepsilon} \textbf{(2.4.1.10)}$$

The effective conductivity is the value that is usually specified in data sheets, although it might be labeled as merely "conductivity." The first term on the right-hand side of the above equation is the static conductivity, and we can define the last term to be conductivity due to an alternating field. Thus

$$\sigma_e = \sigma_s + \sigma_a \textbf{(2.4.1.11)}$$

This last equation highlights the fact that two terms contribute to the loss tangent. The loss due to collisions of electrons with other electrons and atoms.For instance, if the static conductivity is high (copper), then charges flow very easily without many collisions. At first glance it seems strange that a term that approaches infinity in the numerator describes a low loss structure, but it must be remembered that infinite conductivity implies zero electric field (and finite current density). That is, instead of viewing the current density as a function of the electric field,

$$\overline{J_c} = \sigma_s \overline{E} \textbf{(2.4.1.12)}$$

View the electric field as a function of the current density.

(2.4.2) Current Flow in a Coil

When an electric current flows in a coil the growing magnetic field produces induced current which opposes the original growing current. But when the current decays the induced current tends to present this decaying by

producing induced current i in the original direction. The corresponding induced voltage or electromagnetive force V is

$$V = L\frac{di}{dt} \qquad (2.4.2.1)$$

L is called coil inductance

For alternating current with angular frequency ω and amplitude i_o

$$i = i_o e^{i\omega t} \qquad (2.4.2.2)$$

The voltage is given by

$$V = i\omega L\, i_o e^{i\omega t} = V_o e^{i\omega t} \qquad (2.4.2.3)$$

Therefore the coil resistance is given by

$$X_l = \frac{V_e}{i_e} = \frac{V_o}{i_o} = i\omega L \qquad (2.4.2.4)$$

This resistance is known as inductive resistance. The symbols V_e and i_e stands for the effective voltage and current respectively.

(2.5) Energy splitting and Zeeman Effect

The ZeemanEffect is the name for the splitting of atomic energy levels or spectral lines due to the action of an external magnetic field. The effect was first predicted by H. A. Lorenz in 1895 as part of his classic theory of the electron, and experimentally confirmed some years later by P. Zeeman. Zeeman observed

A line triplet instead of a single spectral line at right angles toa magnetic field, and a line doublet parallel to the magnetic field. Later, more complex splitting of spectral lines were observed, which became known as the anomalous

ZeemanEffect. To explain this phenomenon, GoudsmitandUhlenbeckfirst introduced the hypothesis of electron spin in 1925. Ultimately,it became apparent that the anomalous Zeeman Effect was actually the rule and the "normal" Zeeman Effect the exception [67].

The normal Zeeman Effect only occurs at the transitions between atomic states with the total spin S = 0. The total angular momentum $\boldsymbol{J} = \boldsymbol{L} + \boldsymbol{S}$ of a state is then a pure orbital angular momentum ($\boldsymbol{J} = \boldsymbol{L}$). For the corresponding magnetic moment, we can simply say that:

$$\mu = \frac{\mu_B}{\hbar} j \qquad (2.5.1)$$

Where

$$\mu_B = \frac{\hbar e}{-2m_e} \qquad (2.5.2)$$

(μ_B = *Bohr's* magneton, m_e = mass of electron, e = elementarycharge, $\hbar = h/2\pi$, h = *Planck's* constant).

In an external magnetic field $\boldsymbol{B}$, the magnetic moment has theenergy

$$E = -\mu . B \qquad (2.5.3)$$

The angular-momentum component in the direction of themagnetic field can have the values$J_z = M_J \cdot \hbar$ with $M_J = J, J-1, \ldots, -J$

Therefore, the term with the angular momentum J is split in to $2J + 1$ equidistant *Zeeman* components which differ by thevalue of M_J . The energy interval of the adjacent components M_J, M_{J+1} is

$$\Delta E = \mu_B . B \qquad (2.5.4)$$

Where an electron travelling in a circular orbital perpendicular to the Z axis has magnetic momentum μ_{LZ} to the orbital angular momentum L by relation

$$\mu_{LZ} = \frac{e}{2m_e} L_Z \qquad (2.5.5)$$

On the other hand for electron spin it is experimentally observed that

$$\mu_{SZ} = g\frac{e}{2m_e}S_Z \qquad (2.5.6)$$

Where g is lande factor

For an electron has both spin angular momentum, orbital angular momentum and total angular momentum we can write

$$\mu_{JZ} = g_L\frac{e}{2m_e}J_Z \qquad (2.5.7)$$

Where Z component of the total angular momentum

If the magnetic field is in the Z direction

$$\Delta E = -g_L\frac{e}{2m_e}J_Z\,B \qquad (2.5.8)$$

Thus

$$\Delta E = -g_L\frac{eh}{4\pi m_e}m_j\,B$$

$$= -g_L\mu_B m_j\,B \qquad (2.5.9)$$

$\mu_B = 9.274\times10^{-24}$ J/ T is called Bohr magneton.

Then the change in photon energy is

$$\Delta E = g_{eff}\,\mu_B\ B \qquad (2.5.10)$$

g_{eff} is the effective g factor for the transition.

We can observe the normal Zeeman effect e.g. in the red spectral line of cadmium (_λ_0 = 643,8 nm, f_0 = 465,7 THz). Itcorresponds to the transition $^1D_2$ (J = 2, S = 0) → $^1P_1$ (J = 1,S = 0) of an electron of the fifth shell .In the magnetic field, the $^1D_2$ level splits into five *Zeeman* components, and the level $^1P_1$ splits into three *Zeeman* components having the spacing calculated using equation (2.5.4).

Optical transitions between these levels are only possible inthe form of electrical dipole radiation. The following selectionrules apply for the magnetic quantum numbers M_J of the statesinvolved:

$\Delta M_J = \pm 1$ for σ components

$\Delta M_J = 0$ for π components (2.5.11)

Thus, we observe a total of three spectral lines; theπcomponent is not shifted and the two σ components are shifted by

$$\Delta f = \pm \frac{\Delta E}{h} \qquad (2.5.12)$$

$\Delta E = V_m \equiv magnetic\ energy$

With respect to the original frequency. In this equation, $\Delta E$is the equidistant energy split calculated in (2.5.4).

Depending on the angular momentum component ΔM_J in the direction of the magnetic field, the emitted photons exhibit different angular distributions. The angular distributions in the form of two-dimensional polar diagrams. They can be observed experimentally, as the magnetic field is characterized by a common axis for all cadmium atoms [68].

In classical terms, the case $\Delta M_J = 0$ corresponds to an infinitesimal dipole oscillating parallel to the magnetic field. No quanta are emitted in the direction of the magnetic field, i.e.

The π^- component cannot be observed parallel to the magnetic field. The light emitted perpendicular to the magnetic field is linearly polarized, whereby the ***E***-vector oscillates in the direction of the dipole and parallel to the magnetic field

Conversely, in the case $\Delta M_J = \pm 1$ most of the quanta travel inthe direction of the magnetic field. In classical terms, this casecorresponds to two parallel dipoles oscillating with a phase difference of 90^0. The superposition of the two dipoles produces a circulating current. Thus, in the direction of the

magnetic field, circularly polarized light is emitted; in the positive direction, it is clockwise-circular for $\Delta M_J = +1$ and anticlockwise- circular for $\Delta M_J = -1$.

The Zeeman Effect enables spectroscopic separation of the differently polarized components. To demonstrate the shift, however, we require a spectral apparatus with extremely high resolution, as the two π components of the red cadmiumline are shifted e.g. at a magnetic flux density B = 1 T by only Δf = 14 GHz , respectively$\Delta\lambda$= 0,02 nm.

In the experiment a Fabry-Perot etalon is used. This is a glass plate which is plane parallel to a very high precision with both sides being aluminized. The slightly divergent light enters the etalon, which is aligned perpendicularly to the optical axis, and is reflected back and forth several times, whereby part of itemerges each time. Due to the aluminizing this emerging part is small, i.e., many emerging rays can interfere [69].

Behind the etalon the emerging rays are focused by a lens on to the focal plane of the lens. There a concentric circular fringe pattern associated with a particular wavelength can be observed with an ocular. The aperture angle of a ring is identical with the angle of emergence α of the partial rays from the Fabry-Perot etalon.

The rays emerging at an angle of $\alpha_k$interfere constructively with each other when two adjacent rays fulfill the condition for "curves of equal inclination":

$$\Delta = 2d\sqrt{n^2 - \sin^2 \alpha_k} = k.\lambda \quad (2.5.8)$$

((Δ= optical path difference, d = thickness of the etalon,n = refractive index of the glass, k = order of interference)).

A change in the wavelength by δ_λ is seen as a change in thea aperture angle byα Depending on the focal length of the lens, the aperture angle δ_α corresponds to a radius δ_r and the changein the angle δ_λ to a change in the radius δ_r.

If a spectral line contains several components with the distance δ_λ , each circular interference fringe is split into as many components with the radial distanceδ_r. So a spectral line doublet is recognized by a doublet structure and a spectral line triplet by a triplet structure in the circular fringe pattern. The complete experimental setup in transverse configuration is illustrated .Fabry-Perot etalon as an interference spectrometer. The ray path is drawn for an angle $\alpha > 0$ relative to the optical axis. The optical path difference between two adjacent emerging rays is

$$\Delta = n.\Delta_1 - \Delta_2 \qquad (2.5.9)$$

Experimental setup for observing the Zeeman Effectin transverse configuration, the position of the left edge ofthe optics riders is given in cm.

The total intensity of all Zeeman components is the same in allspatial directions. In transverse observation, the intensity of the π component is equal to the total intensity of the two σ components [63].

(2.6) Metal Detection on the Basis of Atomic Spectra

(2.6.1) History and Development

Toward the end of the 19th century, many scientists and engineers used their growing knowledge of electrical theory in an attempt to devise a machine which would pinpoint metal. The use of such a device to find ore-bearing rocks would give a huge advantage to any miner who employed it. The German physicist Heinrich Wilhelm Dove (1803-1879) inventedthe induction balance system, which was incorporated into metal detectors a hundred years later. Early machines were crude, used a lot of battery power, and worked only to a very limited degree. Alexander Graham Bell used such a device to attempt to locate a bullet lodged in the chest of American President James Garfield in 1881; the metal detector worked correctly but the attempt was

unsuccessful because the metal coil spring bed Garfield was lying on confused the detector.[1]

(2.6.2) Modern Developments

The modern development of the metal detector began in the 1920s. Gerhard Fisher had developed a system of radio direction-finding, which was to be used for accurate navigation. The system worked extremely well, but Fisher noticed that there were anomalies in areas where the terrain contained ore-bearing rocks. He reasoned that if a radio beam could be distorted by metal, then it should be possible to design a machine which would detect metal using a search coil resonating at a radio frequency. In 1925 he applied for, and was granted, the first patent for a metal detector. Although Gerhard Fisher was the first person granted a patent for a metal detector, the first to apply was Shirl Herr, a businessman from Crawfordsville, Indiana. His application for a hand-held Hidden-Metal Detector was filed in February 1924, but not patented until July 1928. Herr assisted Italian leader Benito Mussolini in recovering items remaining from the Emperor Caligula's galleys at the bottom of Lake Nemi, Italy, in August 1929. Herr's invention was used by Admiral Richard Byrd's Second Antarctic Expedition in 1933, when it was used to locate objects left behind by earlier explorers. It was effective up to a depth of eight feet. [2]

However, it was one a Polish officer attached to a unit stationed in St Andrews, Fife, Scotland, during the early years of World War II, who refined the design into a practical Polish mine detector. They were heavy, ran on vacuum tubes, and needed separate battery packs.[3]

The design invented by Kosacki was used extensively during the clearance of the German mine fields during the Second Battle of El Alamein

when 500 units were shipped to Field Marshal Montgomery to clear the minefields of the retreating Germans, and later used during the Allied invasion of Sicily, the Allied invasion of Italy and the Invasion of Normandy.[4] As it was a wartime research operation to create and refine it, the knowledge that Kosacki created the first practical metal detector was kept secret for over 50 years.

(2.6.3) Further Refinements

Many manufacturers of these new devices brought their own ideas to the market. White's Electronics of Oregon began in the 1950s by building a machine called the Ore master Geiger counter. Another leader in detector technology was Charles Garrett, who pioneered the BFO (Beat Frequency Oscillator) machine. With the invention and development of the transistor in the 1950s and 1960s, metal detector manufacturers and designers made smaller lighter machines with improved circuitry, running on small battery packs. Companies sprang up all over the USA and Britain to supply the growing demand. Modern top models are fully computerized, using integrated circuit technology to allow the user to set sensitivity, discrimination, track speed, threshold volume, notch filters, etc., and hold these parameters in memory for future use. Compared to just a decade ago, detectors are lighter, deeper-seeking, use less battery power, and discriminate better. Larger portable metal detectors are used by archaeologists and treasure hunters to locate metallic items, such as jewelry, coins, bullets, and other various artifacts buried shallowly underground[4].

(2.6.4) Discriminators

The biggest technical change in detectors was the development of the induction-balance system. This system involved two coils that were

electrically balanced. When metal was introduced to their vicinity, they would become unbalanced. What allowed detectors to discriminate between metals was the fact that every metal has a different phase response when exposed to alternating current. Scientists had long known of this fact by the time detectors were developed that could selectively detect desirable metals, while ignoring undesirable ones.

Even with discriminators, it was still a challenge to avoid undesirable metals; because some of them have similar phase responses e.g. tinfoil and gold, particularly in alloy form. Thus, improperly tuning out certain metals increased the risk of passing over a valuable find. Another disadvantage of discriminators was that they reduced the sensitivity of the machines [15].

(2.6.5) New Coil Designs

Coil designers also tried out innovative designs. The original induction balance coil system consisted of two identical coils placed on top of one another. Compass Electronics produced a new design: two coils in a D shape, mounted back-to-back to form a circle. This system was widely used in the 1970s, and both concentric and D type (andwide scan as they became known) had their fans. Another development was the invention of detectors which could cancel out the effect of mineralization in the ground. This gave greater depth, but was a non-discriminate mode. It worked best at lower frequencies than those used before, and frequencies of 3 to 20 kHz were found to produce the best results. Many detectors in the 1970s had a switch which enabled the user to switch between the discriminate mode and the non-discriminate mode. Later developments switched electronically between both modes [10]. The development of the induction balance detector would ultimately result in the motion detector, which constantly checked and balanced the background mineralization [5].

(2.6.6) Pulse Induction

At the same time, developers were looking at using a different technique in metal detection called pulse induction. Unlike the beat frequency oscillator or the induction balance machines which both used a uniform alternating current at a low frequency, the pulse induction machine simply fired a high-voltage pulse of signal into the ground. In the absence of metal, the pulse decayed at a uniform rate, and the time it took to fall to zero volts could be accurately measured. However, if metal was present when the machine fired, a small current would flow in the metal, and the time for the voltage to drop to zero would be increased. These time differences were minute, but the improvement in electronics made it possible to measure them accurately and identify the presence of metal at a reasonable distance. These new machines had one major advantage: they were completely impervious to the effects of mineralization, and rings and other jewelry could now be located even under highly-mineralized black sand [5].

(2.6.7) Uses

(2.6.7.1) Archaeology

In England and Wales metal detecting is legal provided that permission is granted by the landowner, and that the area is not a Scheduled Ancient Monument, a site of special scientific interest (SSSI), or covered by elements of the Countryside Stewardship Scheme[7].

Items discovered which fall within the definition of treasure must be reported to the coroner or a place designated by the coroner for treasure. The voluntary reporting of finds which do not qualify as treasure to the Portable Antiquities Scheme or the UK Detector Finds Database is encouraged. [5]

The situation in Scotland is very different. Under the Scots law principle of bona vacantia, the Crown has claim over any object of any material value where the original owner cannot be traced. There is also no 300 year limit to Scottish finds. Any artifact found, whether by metal detector survey or from an archaeological excavation, must be reported to the Crown through the Treasure Trove Advisory Panel at the National Museums of Scotland. The panel then determines what will happen to the artifacts. Reporting is not voluntary, and failure to report the discovery of historic artifacts is a criminal offence in Scotland. [6]

(2.6.7.2) As a Hobby

This 156-troy-ounce (4.9 kg) gold nugget, known as the Mojave Nugget, was found by an individual prospector in the Southern California Desert using a metal detector.

There are six major types of hobbyist activities involving metal detectors:

Coin shooting is looking for coins after an event involving many people, like a baseball game, or simply looking for any old coins. Some coin shooters conduct historical research to locate sites with potential to give up historical and collectible coins.

Prospectingis looking for valuable metals like gold and silver in their natural forms, such as nuggets or flakes [8].

General metal detecting is very similar to coin shooting except that the metal detectorist is after any type of historical artifact. Metal detectorists may be dedicated to preserving historical artifacts, and often have considerable expertise. Coins, bullets, buttons, axe heads, and buckles are just a few of the items that are commonly found by relic hunters; in general the potential is far

greater in Europe and Asia than many other parts of the world. More valuable finds in Britain alone include the Staffordshire Hoard of Anglo-Saxon gold, the gold Celtic Newark Torc, the RinglemereCup,West Bag borough Hoard, Milton Keynes Hoard, Roman Crosby Garrett Helmet, Stirling Hoard, Collette Hoard and thousands of smaller finds.

Beach combing is hunting for lost coins or jewelry on a beach. Beach hunting can be as simple or as complicated as one wishes to make it. Many dedicated beach hunters also familiarize themselves with tide movements and beach erosion. There are two main techniques for beach hunting. The first one is called "gridding", which is when you search in a pattern. For example, you start from the beach line, and work your way down to the shoreline, move to the side a little, and repeat the process. The next technique is called "Random searching". Random searching is when you walk around the beach in no particular pattern, hoping to cover more ground.

Metal detecting clubs across the United States, United Kingdom and Canada exist for hobbyists to learn from others, show off finds from their hunts and to learn more about the hobby [9].

(2.6.7.3) Politics and Conflicts in the Metal Detecting Hobby

The metal detecting community and professional archaeologists have differences related to the location, recovery and preservation of historic finds and locations. Archaeologists claim that detector hobbyists take an artifact-centric approach, removing these from their context resulting in a permanent loss of historical information. Archaeological looting of places like Slack Farm in 1987 and Petersburg National Battlefield serve as evidence against allowing unsupervised metal detecting in historic locations [10].

Hobby detectorists often state that professional Archaeologists' resource limitations results in the loss or damage of many artifacts by plows, development, erosion and livestock. The language and breadth of legislation regarding artifact collection is also an issue, as the Archaeological Resources Protection Act of 1979excludes scattered coins, the main target of inland hobby detectorists. Many detectorists take issue with the breadth of metal detecting bans, marking large swaths of property off-limits which are either well-documented already or unlikely to ever receive professional attention. Suggestions to certify or offer limited permits for detecting at historic sites have been attempted in some areas of the United States [11].

Recently, productive efforts for cooperation between professionals and metal detecting hobbyists have begun, including the Montpelier Archaeology Project and BRAVO Battlefield Restoration and Archaeological Volunteer Organization and many more. In these programs, skilled detectorists work with experienced professionals with common goals of accurate, efficient site discovery and excavation. Away from supervised sites, hobbyists using improved record keeping and employment of Global Positioning System, GIS, logbooks, photo scales and online databases may aid professionals in evaluating possible sites. When searching for a site, detectorists can aid with electronic scanning, reducing the need for test holes. Some land managers, such as The Tennessee Valley Authority have cited a role for Amateur Archaeologists in protecting sensitive sites from illegal looting and metal detector hobbyists have aided in the location and preservation of many sites [12].

(2.6.7.4) Security Screening

A series of aircraft hijackings led the United States in 1972 to adopt metal detector technology to screen airline passengers, initially using

magnetometers that were originally designed for logging operations to detect spikes in trees. The Finnish company Outokumpu adapted mining metal detectorsstill housed in a large cylindrical pipe, to make a commercial walk-through security detector. The development of these systems continued in a spin-off company and systems branded as Metor Metal Detectors evolved in the form of the rectangular gantry now standard in airports. In common with the developments in other uses of metal detectors both alternating current and pulse systems are used, and the design of the coils and the electronics has moved forward to improve the discrimination of these systems. In 1995 systems such as the Metor 200 appeared with the ability to indicate the approximate height of the metal object above the ground, enabling security personnel to more rapidly locate the source of the signal. Smaller hand held metal detectors is also used to locate a metal object on a person more precisely. [7]

(2.6.7.5) Industrial Metal Detectors

Industrial metal detectors are used in the pharmaceutical, food, beverage, textile, garment, plastics, chemicals, lumber, and packaging industries.

Contamination of food by metal shards from broken processing machinery during the manufacturing process is a major safety issue in the food industry. Metal detectors for this purpose are widely used and integrated into the production line.

Current practice at garment or apparel industry plants is to apply metal detecting after the garments are completely sewn and before garments are packed to check whether there is any metal contamination (needle, broken needle, etc.) in the garments. This needs to be done for safety reasons.

The industrial metal detector was developed by Bruce Kerr and David Hiscock in 1947. The founding company Goring Kerr pioneered the use and development of the first industrial metal detector. Mars Incorporated was one of the first customers of Goring Kerr using their Met locate metal detector to inspect Mars bar [8].

(2.6.7.6) Basic Operation

The basic principle of operation for the common industrial metal detector is based on a 3 coil design. This design utilizes an AM (amplitude modulated) transmitting coil and two receiving coils one on either side of the transmitter. The design and physical configuration of the receiving coils are instrumental in the ability to detect very small metal contaminates of 1mm or smaller. Today modern metal detectors continue to utilize this configuration for the detection of tramp metal.

The coil configuration is such that it creates an opening whereby the product (food, plastics, pharmaceuticals, etc.) passes through the coils. This opening or aperture allows the product to enter and exit through the three coil system producing an equal but mirrored signal on the two receiving coils. The resulting signals are summed together effectively nullifying each other[11].

When a metal contaminant is introduced into the product an unequal disturbance is created. This then creates a very small electronic signal that is amplified through special electronics. The amplification produced then signals a mechanical device mounted to the conveyor system to remove the contaminated product from the production line. This process is completely automated and allows manufacturing to operate uninterrupted [12].

(2.6.7.7) Civil Engineering

In civil engineering, special metal detectors (cover meters) are used to locate reinforcement bars. These detectors are less sophisticated, and can only locate metallic objects below the surface.

Chapter Three

Literature Review

(3.1) Introduction

Many attempts were made to construct metal detectors using magnetic or electric or electromagnetic fields [66].

Attempts are also made to use quantum conductivity for metal characterization and detection [13].

This chapter is concerned with exhibiting some of them.

(3.2) Construction of a Beat Frequency Oscillator Metal Detector

There are threeprimary technologies in use by metal detectors today. One of them is known as very low frequency (VLF) detectors work by producing a relatively low frequency (5-50 kHz) time-varying magnetic field with a large (6-12 inch) inductor. A second, smaller coil is shielded from detecting any direct fields induced by the first coil, and is tuned to listen for possible fields due to eddy currents generated by nearby metal objects.

The second is known as Pulse Induction detectors work much like SONAR on a submarine. Electric current is sent in microsecond long pulses through a coil of wire that causes a brief magnetic field to be induced. If this pulse hits a meal object, it is reflected back to the coil of wire, which measures the reflected pulse. While pulse induced detectors aren't very good at determining different types of metal, their effective working depth is much greater than that of a VLFdetector.

The third technique is the beat frequency oscillator (BFO) style detector works by comparing two different frequency oscillators in order to detect meal objects. The large search head coil is tuned to match the frequency of a reference oscillator, typically located inside the control box. As the head is swept over metal objects, the inductance of the head changes, causing a frequency shift in the oscillating circuit,as the two frequencies change in reference to each other, some simple circuitry alerts the operator that there is nearby treasure [14].

Initially, it seems the beat frequency oscillator detector will be the best choice to build due to its relatively simple circuitry, which will allow us to focus more on the electromagnetic theory during the project.

DESIGN AND CONSTRUCTION

Two inductors that are used to detect the presence of a metal, one inductor is used as a reference coil with specific known inductance. This was constructed by winding a 120 turns of 34 AWG wire around a0.5wooden dowel. When placed in an RLC circuit, it will oscillate at a given frequency. A second inductor (the search coil) is used to detect the presence of metal. Our search coil consisted of a 12 inch non-conducting loop wrapped with 8 turns of 34 AWG wire.

This search coil's inductance and resonant frequency is found by circuit theory to be:

$$\sqrt{lc} = 1$$

This frequency is then closely matched with the reference coil by the fine tuning of the reference coil; it is tuned by screwing or unscrewing a metal washer around the reference coil until the frequencies are about the same. Once there are two oscillating RLC circuits, closely matched, one can slightly alter the search coil's inductance then compare the difference between them [22].

Altering the search coil's inductance is accomplished by placing a large metal object near the search coil; this will in turn change the frequency at which this RLC circuit is oscillating. Now that the two circuits are oscillating at different frequencies, this frequency difference can beanalyzed, stepped down and amplified into an audible toneutilizing a high impedance speaker or headphones. If there is a large difference between the frequencies, this will produce a higher frequency on the audio output. However, when the

frequencies are still very close together, a small beat, or no beat will be output to the audio.

Using this method, there will always be a tone produced regardless of the presence of metal. This is due to the fact that these two circuits will never be exactly the same because it is very; very difficult to practically match the inductors completely, so they will be oscillating at slightly different frequencies. There will always be a slight difference between the two resonant frequencies regardless of how closely one tries to match them. However, if the frequencies change noticeably, then so will the tone being produced. So, while there will always be a small tone being produced, a noticeable changing tone means there is metal being detected [25].

When analyzed on an oscilloscope, the audio output is seen to be periodic spikes in voltage when a frequency difference is present in the two RLC circuits. The larger the difference between the frequencies, the wider the pulse becomes. However, this spike's width is rather smallbecause the frequencies never change considerable around any small piece of metal, which makes this pulse rather difficult to hear using a speaker or headphones [23].

DISCUSSION

The original design goals were to be able to detect a small piece of metal, such as a coin, buried under approximately two inches of dirt. Unfortunately, after construction and initial testing, it was found that the metal detector was simply not that sensitive. In fact, it took a noticeably large amount of metal (on the order of 1-2 kg) in order to change the search coil's inductance enough to produce a noticeable beat. A variety of search coils were tested, ranging from 7 inches to 12 inches, and ranging in inductance values (12-108) nH. Unfortunately, the B-field produced by these inductors was simply not large

enough to induce any eddy currents in small pieces of metal.Our final circuit model oscillated at 104 kHz. Bringing a large piece of metal close to the search coil resulted in an inductance that changed the coil's resonance to 107 kHz, producing a 3 kHz beat. Unfortunately, the audio driver portion of our circuit didn't perform as well as could havebeen hoped, so we found it much more functional to use an oscilloscope to observe the beat change. Perhaps we could have used a simple LPF integrator circuit to drive a needle-point meter as a better way to alert the user as to the presence of metal.

(3.3) INDUCTION BALANCE METAL DETECTOR

The design described here works on inductionBalance (IB) or the TR principle (Transmit-Receive).

In the usual circuit for a metallocator,A search coil, usually 6in or so in diameter is connected in the circuit to oscillate at between 100-150 kHz. A second internal oscillator operating on the same frequency is included and a tiny part of each signal is taken to a mixer and a beat note is produced. When the search coil is brought near metal, the inductance of the coil is changed slightly, altering the frequency and thus the tone of the note. A note is produced continually and metal is identified by a frequency change in the audio note.

The IB principal uses two coils arranged in such a way that there is virtually no inductive pick-up between the two. A modulated signal is fed into one.

A really sensitive design operating is based on induction balance circuit will really sniff out those buried coins and other items of interest at great depths depending on the size of the object.

The electromagnetic field is disturbed and the receiver coil picks up an appreciably higher signal. The circuit is therefore arrangedso that the signal is gated and is set up so that only the minutest part of the signal is heard when no metal is present. When the coil is near metal, only a minute change in level becomes an enormous change in volume.BFO detectors are not as sensitive as IB types and have to be fitted with a Faraday screen toreduce capacitive effects on the coil [30].

(3.4)Active Induction Balance Method for Metal Detector Sensing Head utilizing Transmitter-Buckingand Dual Current Source

Electromagnetic induction (EMI) sensors have been used for the detection of metallic parts of landmines since the World War II and are nowadays considered a rather mature technology [1].

However, in spite of recent developments in other landmine detection techniques, EMI sensors still remain an area of active research, [2]. Due to their sensitivity, robustness and high-speed operation, they are practically the only sensors that are currently used in humanitarian demining for close-in detection in the field [1], [2].

Time-domain (TD) or pulse induction (PI) EMI sensors transmit a primary magnetic field of pulsewaveform and detect a weak secondary field induced by eddy-currents in the metallic object after the transmitter has been shut-off. Since the receiver responses corresponding to the primary and the secondary field are separated in time, TD sensors are inherently balanced which greatly simplifies sensor design. However, their fundamental limitation is the available excitation spectrum band (i.e. the equivalent time frames that eventually cannot capture ‘very early’ or ‘very late’ time data) [2].

Frequency-domain (FD) EMI sensors provide better control over the power and frequency content of the excitation spectrum. Also, they generally claim higher sensitivity and improved SNR (signal-tonoise)response in metal detector applications when compared to TD sensors. [2].

On the other hand, in order to explore their benefits an efficient method of primary field suppression (induction balance, IB) must be provided. There are several IB methods that are normally used for design of FD EMI sensors: physical separation of transmit (TX) and receive (RX) coils [3], RX coils in gradiometer configuration, overlapping TX and RX coils (OO and DD types) [4], orthogonal coil arrangement, etc.

All of the above IB implementations have some apparent drawbacks when it comes to design ofsensing head for a handheld landmine detector with additional model-based metal characterizationfeatures. Such sensor needs to have simple and compact geometry, high detection sensitivity, highspatial resolution and pinpointing accuracy. It also must provide good invariability of the measureddata so that the parameters of a model can be reliably computed. Based on these requirements, a sensing head configuration based on the transmitter-bucking approach is proposed [3].

Sensing Head Design

The initial parameter for the design of a landmine detector sensing head is the diameter of its maintransmitter coil $D1$ which can be used as a rough estimate of the sensor's maximum ground penetration depth [2]. Having in mind the practical requirements of landmine detection, we set $D1$ at 30 cm. Other geometrical properties of the sensing head (coil diameters and number of turns) are obtained from $D1$ and the given mathematical model of the chosen coil configuration.

The transmitter stage consists of two concentric coplanar coils (TX1 and TX2) driven by AC current of opposite direction so as to create a central region in which the receiver coil senses zero primary field, figure 1. If a circular current loop approximation is used for both TX1 and TX2 coils, the expression for vertical component of magnetic field *BZ* as a function of radial distance *r* from the coil. [3]

In general, very careful coil design and high precision in the production of a sensing head are needed for practical application to landmine detection. Laboratory function generator (Voltcraft VG-506) was used as a reference voltage source in the experiments. Voltage induced in RX coil, F*u*, was fed to unity-gain instrumentation amplifier and measured with an oscilloscope. As a proof of AIB concept, F*u* was measured at different frequencies (absolute value and normalized to *u*IB) for a balanced sensor with passive IB (I_1=I_2) and with AIB. The excitation current magnitude was set to 0.5A. Active balance was adjusted separately for each frequency. The results clearly indicate that the imbalances of the passive IB can be effectively compensated with AIB. Additional experiments are needed in order to fully characterize the method.

For a design of novel, frequency-domain EMI landmine detector with additional model-based metalcharacterization features, a sensing head configuration based on the transmitter-bucking approach was used. For this configuration, the induction balance problem in terms of balancesensitivity to small perturbations of geometrical properties of the sensing head was analyzed. The obtained results suggest that although the overall IB sensitivities are quite low, the total sensor imbalances expressed in absolute terms can become significant, therefore complicating the sensor design. In order to overcome this limitation and to explore new methods of coping with soil effects on IB, experimentally verified a prototype sensor with dual current source and active induction balance scheme was developed.

(3.5) Quantum Conductivity for Metal-Insulator-Metal Nanostructures

The traditional approach for understanding of nanoplasmonic systems problems involves comprehensive electromagnetic simulations of the nanostructures using classical expressions for the dielectric response of the materials. The optical or purely electromagnetic properties of plasmonic structures for a wide range of applications have been studied in many publications [1-15]. The classical approach has worked well for many systems whose dimensions are greater than a few nanometers. However, there are proposed systems and applications where the minimum feature sizes are reduced below a nanometer. This situation has triggered greater scrutiny of the assumptions underlying the classical treatment of plasmons.

To overcome the limitations inherent in the classical nanoplasmonic analysis a sub-field of nanophotonics, sometimes referred to as quantum plasmonics, recently emerged. One branch of this sub-field explores the quantum tunneling of electrons between nanostructured metals (plasmonics) that are separated by insulator materials. The quantum techniques range from numerically intensive time-dependent density functional theory to a simple Quantum Correction Model that computes a linewidth factor or spatial dispersion models; the latter approaches are based on the Drude model [16-22]. While electron tunneling is driven by electromagnetic fields, charge exchange limits field enhancement in the gap region between the two metals. In contrast, the purely classical models predict an ever increasing local field enhancement as the gap is reduced. Recent papers in quantum plasmonics have explored the effect of electron tunneling due to metal dimers in vacuum.

This work is related to the literature developed for metal-insulator-metal (MIM) structures [23-36]. A quantum mechanical model is applied that describes tunneling with an applied time-dependent field. Then a set of

frequency-dependent quantum conductivity coefficients is extracted for the nanoplasmonic system. By applying standard quantum mechanical techniques the ac or dc currents enabled via the electron tunneling effect can be estimated by endowing the insulator volume with a set of quantum conductivity functions. This approach is called the Quantum Conductivity Theory (QCT) and it can be applied to nanoplasmonic systems composed of different metals and having different insulator materials separating the metals. Nonlinear quantum conductivity coefficients will enable harmonic generation and two-photon absorption-like phenomena. QCT can be incorporated into computational electromagnetic models in a straightforward fashion, as we demonstrate in this section.

To illustrate how the quantum conductivity affects electromagnetic scattering in nanosystems a system of metal dimers is considered. One applies QCT to two geometries of gold dimers immersed in different media with a variable gap between the metal structures. When vacuum surrounds the dimers the results are compared to available simulation data. To establish the versatility of QCT one embeds the gold dimers in insulators and the results are strikingly different. One also examines the case of a sodium dimer in vacuum for comparison with recent results and the sodium dimer system is used to demonstrate that nonlinear effects also contribute to diminishing the field enhancement. QCT modifies both the linear and nonlinear absorption of the electromagnetic fields and generates harmonic fields.

The current maps bear out that the current saturates as the gap size vanishes. When the space separating the metals is a vacuum the potential barrier is highest and so the range of current density values also spans many decades over the span of gap sizes. Titanium12dioxide has a high electron affinity and the range of current values for the same span of gaps is greatly

reduced; furthermore, the dependence of the current on the gap distance is much weaker.

Similarly, the linear ac conductivity coefficients for gold electrodes with three different insulating layers sandwiched between them have maps that vary over a large range of values; however, very small values of the conductivities have no discernible effect on the electromagnetic field. It is not until the distance is on the order of a nanometer that the quantum properties become important enough to measurably affect the electromagnetic field; one finds that these values of the quantum conductivity are of order 0.1 S/m. The gap distance for such values is around 1 nm for the cases with vacuum and silica, but it extends to larger gap sizes in the titanium dioxide case. The range of conductivities, as seen in the color bars on the right of each map, is much smaller when the insulator is titanium dioxide. As mentioned previously, this is due to the large electron affinity of titanium dioxide.

Maps of the logarithm (base 10) of the linear ac conductivity,) 1(ωσ, versus applied voltage and gap thickness for three cases: (a) Au/vacuum/Au, (b) Au/SiO_2/Au and (c) Au/TiO_2/Au were studied. The units of the linear conductivity are S/m.

There are two non-vanishing nonlinear conductivity coefficients in MIM systems made from the same metals. They are the TPA conductivity and the third harmonic generation (THG) conductivity coefficients. Over the range of wavelengths used in the plots, the conductivities show a relatively weak dependence on wavelength across the visible to mid-wave infrared regions when the gap size is small. The results with the dimer immersed in titanium dioxide are quite distinct from the other two host insulators; the minimum values of the conductivities are twenty orders of13 magnitude larger in TiO_2, but the maxima are smaller by a few orders of magnitude. Most of the differences are directly attributable to the difference in the electron affinity for

the three cases, although the dielectric constants play a role in the observed trends too.

The application of the quantum conductivities requires endowing the space between the metals with its physical properties. The following simple prescription can be adopted from different directions for assigning the quantum conductivities across the insulator. It is convenient and simple to implement, but not the only way. The gap between two metallic nanostructures is the key parameter for determining the distribution of conductivities. The distance from one point to another on two neighboring metal surfaces can be adopted as an estimate of the quantum conductivities along that line. one assumes the following assignment for simple dimers. Lines canbe extended from one metal to another along the symmetry axis; they form annulus-shaped shells in which with quantum conductivities in each shell is determined by the gap distance from one metallic boundary to the other. The width of the annulus is small compared to changes in the quantum conductivity with gap distance. When the gap becomes large enough the quantum conductivities become so small that electronic tunneling is negligible.

Using this procedure several applications of the QCT to nanosystems are considered and we compare our results to relevant literature where possible. The first example is a three-dimensional system of gold cylinder dimers. The total length of the gold cylinder is 100 nm and its radius is 5 nm. There is a gap cut out of its center and the gap is varied between 0.2 nm and 5 nm; the gap is vacuum filled. A plane electromagnetic wave with the electric field parallel to the cylinders' axis impinges on the antenna .The quantum conductivity for gold-vacuum-gold dimer is applied in the gap region and the conductivity is zero outside the gap [46].

The gap impedance can be straightforwardly *gap*sis the gap dielectric constant in the classical limit is also constant in the gap region and taken as zero outside the gap. The voltage divider rule is applied in the receiving mode of the antenna in order to derive the voltage drop across the gap in the presence of an input plane wave polarized along the antenna axis with electric field amplitude. where the open circuit voltage depends on the effective antenna length, defined as in [46].versus gap separation and photon energy. For comparison the classical model results and the quantum corrected results .The field enhancement is red shifted and continually increases in magnitude as the gap goes to zero. The QCT results also have a red shift as the gap decreases, but the enhancement factor has a maximum at a finite gap size. The field enhancement maximum is similar in size and value with that reported by Esteban et al. [19]. In our case it occurs at a gap of 0.7 nm and the field enhancement maximum value is 420 at photon energy 2 eV. The field enhancement data that follow are summarized in Table 2. The gap in our calculations is somewhat longer than the value of 0.5 nm found in Ref [19] and could be attributed to differences in the geometry of the dimers.

Field enhancement map for gold 3D cylinder dimers with a vacuum gap, (a) The cylindrical, center-fed nanoantenna geometry; (b): The classical electromagnetic model; (c) the QCT applied to the vacuum gap.

Next we consider two parallel, infinitely long, gold cylinders. A plane wave is polarized with the electric field parallel to symmetry axis passing through the centers of the two cylinders and it is incident from the side perpendicular to that axis. Linear and nonlinear conductivities in the gap region are assigned by adopting a simple methodology. We draw straight lines connecting the two gold nanoparticles along the symmetry axis, as illustrated. The conductivities on that line are assigned according to its length by identifying the length with the gap parameter; near the symmetry axis the

conductivity is highest and so is the tunneling current, which is illustrated as a thick line .The line thickness becomes thinner indicating that the current drops off as the effective gap widens.

A 2D Comsol finite element solver is used to generate through 10, where the field enhancement is mapped for the gold dimer in vacuum and embedded in two different insulators. The field enhancement for the three cases shows several resonance peaks due to plasmon hybridized excitations [48]. In the hybridation scheme the symmetric resonances are strongly red shifted as the gap is decreased. The peak field enhancement of 420 occurs for the lowest energy hybrid resonance at 2 eV for a gap of 0.7 nm. The field enhancement is quenched below 0.5 nm. Our smallest gap in the figures is 0.2 nm.

Enhanced field maps for gold 2D dimer cylinders embedded in vacuum. The cylinder radii are 10 nm. (a) An illustration of a simple method for assigning linear and nonlinear conductivities in the gap region. The quantum conductivity values are assigned along a straight line connecting the cylinders; and the length of the line is set to the corresponding gap parameter. The current is viewed as flowing along the lines connecting the two particles so that thicker arrows show greater current flow that tapers off at the edges due the lower conductivity. (b) Map of the field enhancement using the classical approach. (c) Field enhancement map using QCT. The minimum gap separation is 0.2 nm.

For the gold dimer in vacuum the lowest energy hybrid resonance displays the same general characteristics as found with the gold nanoantenna in Figure 7. The peak field enhancement is red shifted as the gap parameter is reduced forthe gold dimer embedded in silica, the resonances are shifted to lower energies due to the dielectric constant of the medium. In this case, even though the electron affinity of silica is small, the peak of the field

enhancement is 263 at d=0.45 nm and photon energy 2.3 eV. This is a shorter gap parameter than found for the case of the gold dimer in vacuum. Enhanced field maps for gold 2D dimer cylinders embedded in silica.

For the gold dimer embedded in titanium dioxide the resonance energies are the lowest of the three cases. The multiple resonance structure is retained and the field enhancement is responsible for reducing the potential barrier which increases the quantum ac conductivity. The peaks in the enhancement occur at the edge of our separation boundary of 0.2 nm. The peak value of the field enhancement is 210 at the photon energy 1.7 eV for the second hybridation resonance at a gap parameter at 0.3 nm .The maximum field enhancement is lower than one observed for the other cases, but the value depends on the dielectric function of the gold, which is highly dispersive. The lowest energy resonances are found for the gold dimer in titanium dioxide; this is a consequence of the dielectric constant being the largest for titanium dioxide Enhanced field maps for gold 2D dimer cylinders embedded in titanium dioxide.

For the next sample one applies QCT to the same two-dimensional dimer geometry but now the cylinders are made of sodium. For this study we only consider the vacuum environment.

The general characteristics of these physical quantities are similar to the results for gold cylinders. However, sodium has a smaller work function which increases the corresponding dc current densities for the same gap and applied voltage. The smaller work function also produces correspondingly larger quantum conductivities, as well. Ultimately we examine its effect on the electromagnetic properties of the nanostructures.

The sodium quantum conductivities are applied to the two-dimensional system of sodium cylindrical nanowires with radius r = 4.9 nm. A plane wave with electric field oriented along the dimer axis impinges on the nanoparticles'

system. The results for the field enhancement at the center of the gap under two different situations are presented. The field enhancement in the linear regime, i.e., with low input intensities, for a range of photon energies and gap separations is reported. The peak field enhancement is 55 at the photon energy of 3.22 eV and the gap is 1.1 nm. The results reported by Teperik et al. [22] using time-dependent density functional theory are similar with a field enhancement peaks near 80 at a photon energy near 3 eV with the gap near 0.6 nm. The gap is somewhat larger than found in their study; the difference may be due to a discrepancy in the value of the work function.

Applying the quantum theory of tunneling for MIM structures we derived a set of linear and nonlinear quantum conductivities that can be employed to predict optical properties of Nano scale plasmonic systems. All physical parameters used in our calculations are extracted from the literature and no additional assumptions or fit parameters are required. Furthermore QCT can provide results for any combinations of metals and insulators, and will enable the design of complex device structures with optimized electromagnetic performance. The quantum conductivities also predict new, nonlinear optical effects, which could be exploited in developing future photonic devices.

Using QCT one derives three new nonlinear ac conductivities that can be detected in carefully designed experiments. The description of nonlinear coefficients can be extended to higher harmonic generation to study its efficiency for EUV production, as well. As a validation of QCT we demonstrated how the linear ac conductivity reduces the field enhancement, which compared favorably with results using different methods that were recently reported in several publications [18-22]. Our nonlinear quantum conductivity for two-photon absorption affects the electromagnetic field in the same way as the linear ac conductivity. Our TPA conductivity coefficient

suppresses the field enhancement as the electromagnetic irradiance is increased and it has a similar magnitude to that reported from numerical calculations [18]. In addition one also predicts a third-harmonic field can be generated from the quantum tunneling effect. The second-harmonic coefficient vanishes for dimers made with the same metals and no applied field breaks the symmetry, but by breaking this symmetry though a second-harmonic dipolar field can be generated. The third-harmonic term is nonzero for all combinations of metals, insulators and applied field. Future studies need to explore nonlinear phenomena in greater detail.

(3.6) Zeeman Effect and Statistical Theoretical Model

The Zeeman Effect is the name given to the splitting of the energy levels of an atom when it is placed in an externally applied magnetic field. The occurs because of the interaction of the magnetic moment μ of the atom with magnetic field **B** slightly shifts the energy of the atomic levels by an amount

$$\Delta E = -\mu B \quad (3.6.1)$$

This energy shift depends on the relative orientation of the magnetic moment and the magnetic field.

Nuclear magnetic resonance (NMR) and electron spin resonance (ESR) both depend on the Zeeman splitting of a single energy level within the atom. The first order perturbation theory gives a corresponding energy shift by:

$$\Delta E = \mu_B g_s M_J H \quad (3.6.2)$$

Where

M_J : is orbital angular momentum

g_s : is g-factors (Lande)

In the optical Zeeman Effect atoms are excited to level above the ground state by, collisions with electrons in an electrical discharge .when they return to the ground state, they emit by extra energy as a visible photon whose energy corresponds to the difference in energy between the excited and ground state [33].

According to Maxwell distribution the density of particles is given by

$$n = n_o e^{\frac{E}{\overline{E}}} \quad (3.6.3)$$

Where $\overline{E}$ stands for the uniform energy.

Assuming the oscillating frequency is uniform, then $\overline{E} = hf$

Therefore equation (3.6.3) becomes

$$n = n_o e^{\frac{-E}{hf}} \quad (3.6.4)$$

It is quite natural to assume that the density of photons is proportional to the exited atoms or electrons density i.e.

$$n_p = C_0 n = C_0 n_o e^{\frac{-E}{hf}} \quad (3.6.5)$$

By neglecting kinetic term, when the potential is very high in this case

$$E = -V_0 \quad (3.6.6)$$

Therefore equation (3.6.2) becomes

$$n_p = C_0 n_o e^{\frac{V_0}{hf}} \quad (3.6.7)$$

$$\frac{V_0}{h} \sim \frac{10^{-5}}{r_0}$$

For $r_0 \sim 10^{-5} m \; \frac{V_0}{h} \sim 1 (3.6.8)$

The light intensity of emitted photons is given by

$$I = Cn_p = CC_0 n_o e^{\frac{V_0}{hf}} = I_0 e^{\frac{V_0}{hf}} (3.6.9)$$

By a suitable choice of (3.6.8) and using (3.6.9) parameters one can choose

$$I = I_0 e^{\frac{1}{f}}$$

$$I_0 = 10 (3.6.10)$$

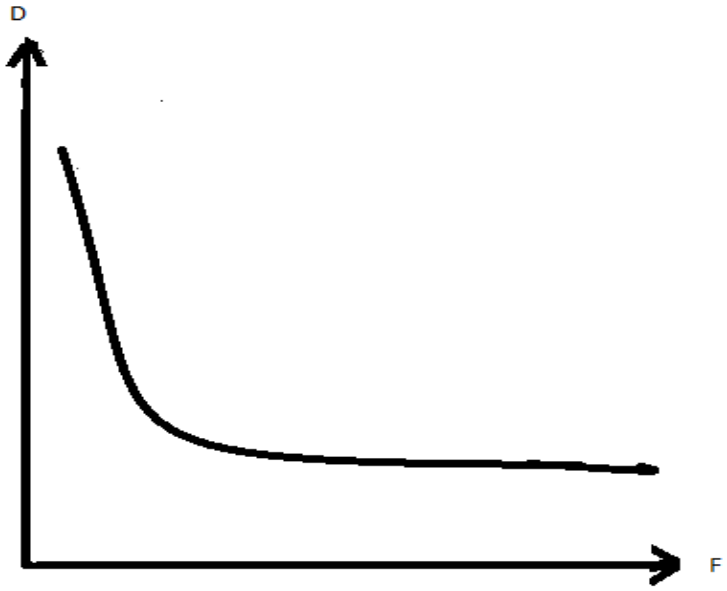

Fig (3.6.1) Theoretical relation between frequency (f) and Intensity (I)

Chapter Four

Identification of Minerals by Electric Coil Detector

(4.1) Introduction

In this work a simple electric detector made of transmitter and receiver coils was designed. The conductivity of the tested metals was used as finger prints that identify minerals. The design of this detector, beside the working principle are exhibited in this chapter. The experimental methodology, beside tables, figures, results, discussion and conclusion are all included in this chapter.

(4.2) Apparatus

The following apparatus were used in the experiments

-10 Resistors (10kΩ, 2.2GΩ, 39kΩ).

-12 Capacitors (0.1μF, 0.01μF, 220μF).

- 6 Transistors (NPN).

-2 Coils (400,500, 600, 700, 1000) rp.

-Wires connection.

-Speakers.

-Cathode Ray Oscillator.

-Board connection.

- Battery (9V).

-A pieces of metal (Cu, Al, Fe, Au, Ag, Sn).

-Signal generator.

(4.3) Method

The metal detector circuit is shown in fig (4.1). It consists of transmitter coil and receiver coil. The transmitter coil current is varied by using signal generator. The emitted photons are allowed to incident on the sample. The sample absorbs photons and re emits them. The signals appearing at oscilloscope were taken before mounting the sample and after mounting it to emit photon emission. The frequency and the corresponding conductivity of samples are recorded and determined from signal generator, current, voltage, the length and cross sectional area of samples. The current and voltage gives resistance, which allows conductivity determination from the dimensions of the sample.In this experiment a transmitter coil emits electromagnetic waves.These electromagnetic waves are allowed to incident on certain materials. The re emitted electromagnetic waves are receipted by a receiver.

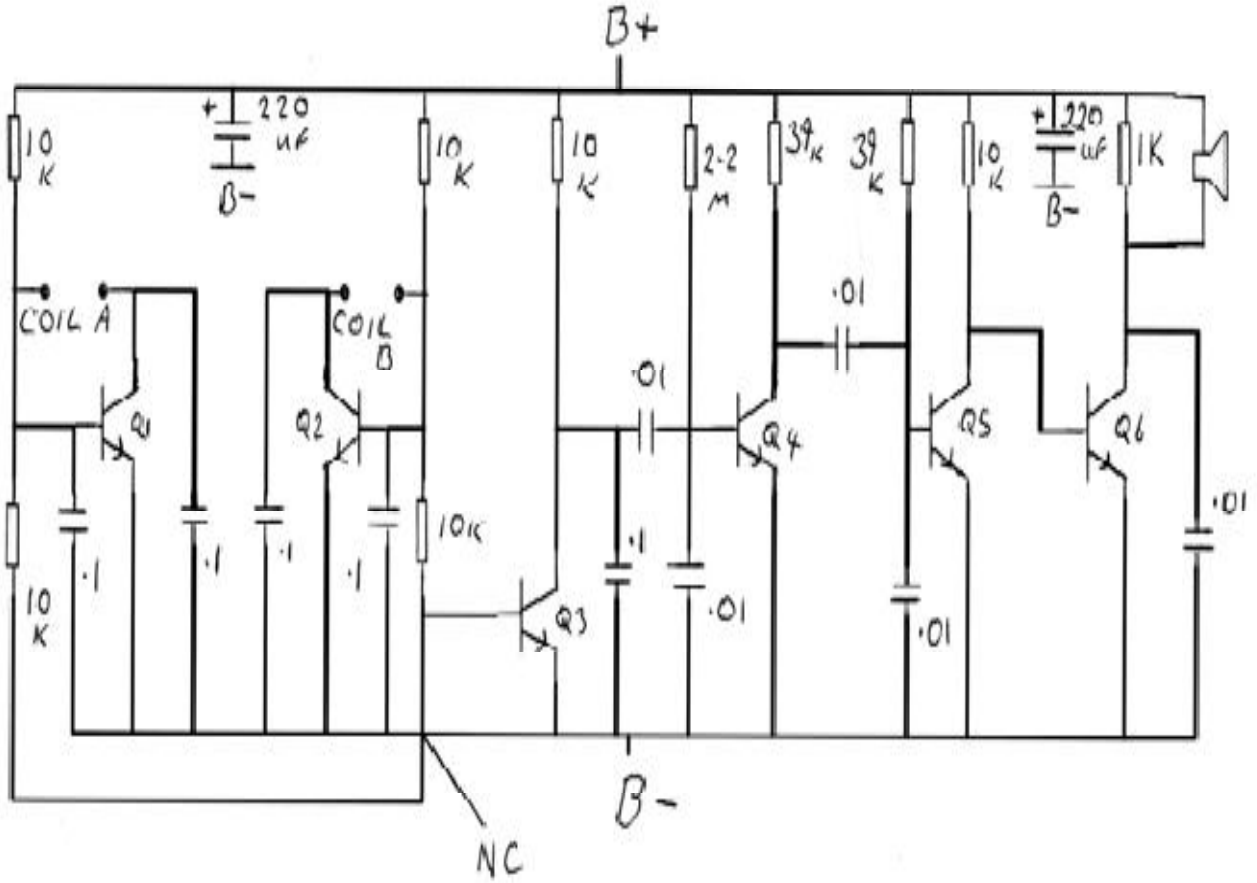

Fig (4.1) Circuit Diagram of Metal Detector

(4.4) Tables and Figures

The following tables and figures relate the amplitudes, frequencies, and conductivities of the received signals for different samples before and after applying magnetic fields.

Table (4.4.1)The Amplitude and frequency of thereceived signal without samples

No of reading	Amplitude\mv	Frequency\Hz
1	180	217.39
2	200	100
3	400	71.4

Table (4.4.2)The signal after the sample (Al) was put between transmitter and receiver

No of reading	Amplitude\mv	Frequency\Hz
1	170	217
2	190	125
3	440	75

Table (4.4.3)The signal after the sample (Fe) was put between transmitter and receiver

No of reading	Amplitude\mv	Frequency\Hz
1	100	192.3
2	180	111
3	520	73.5

Table (4.4.4)The signal after the sample (Cu) was put between transmitter and receiver

No of reading	Amplitude\mv	Frequency\Hz
1	160	208.3
2	170	90.9
3	360	73.5

Table (4.4.5)The signal after the sample (Au) was put between transmitter and receiver

No of reading	Amplitude\mv	Frequency\Hz
1	150	200
2	220	87
3	560	69.4

Table (4.4.6) Relation between frequency (f) and Conductivity (σ) without applied magnetic field for Cu, Al, Fe, Au, Ag, Sn

Frequency (Hz)	Conductivity (10^6 cm.Ω)
24	0.452
27	0.596
29	0.0993
34	0.0917
50	0.143
56	0.337

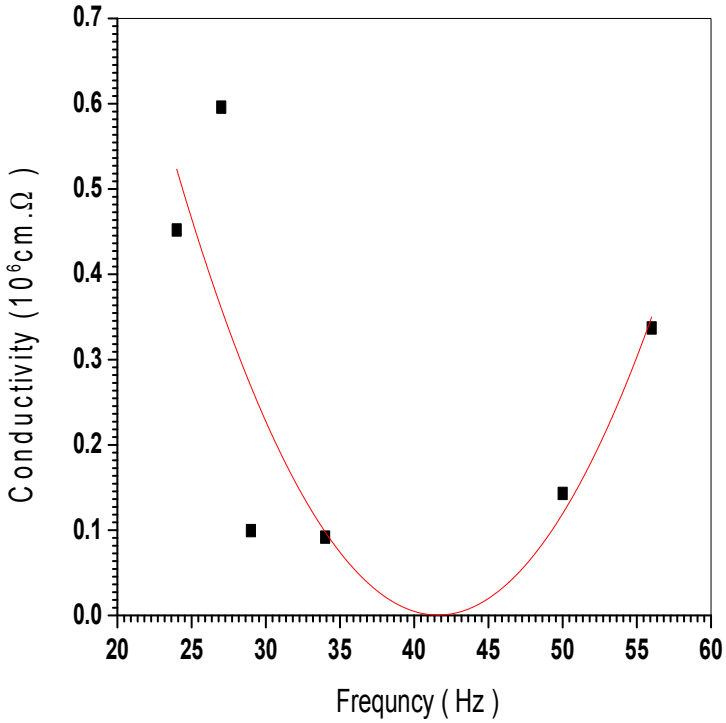

Fig (4.4.1) Relation between resonance frequency and Conductivity for Cu, Al, Fe, Au, Ag, Sn

Table (4.4.7) Relation between frequency (f) and Conductivity (σ)for different magnetic flux densities for gold

Frequency (Hz)	Conductivity (10^6cm.Ω) In 97.3 μT	Conductivity (10^6cm.Ω) In 77.μT	Conductivity (10^6cm.Ω) In 116.7 μT	Conductivity (10^6cm.Ω) In 136.2μT	Conductivity (10^6cm.Ω)In 194.53 μT
55.25746	0.50026	0.12637	0.04739	0.15165	0.06824
47.48594	0.26365	0.03724	0.01396	0.04468	0.02011
40.49329	0.16368	0.03439	0.0129	0.04126	0.01857
35.4219	0.24726	0.05362	0.02011	0.06435	0.02896
26.8109	0.39107	0.1695	0.06356	0.2034	0.09153
24.81177	0.58753	0.2235	0.08381	0.2682	0.12069

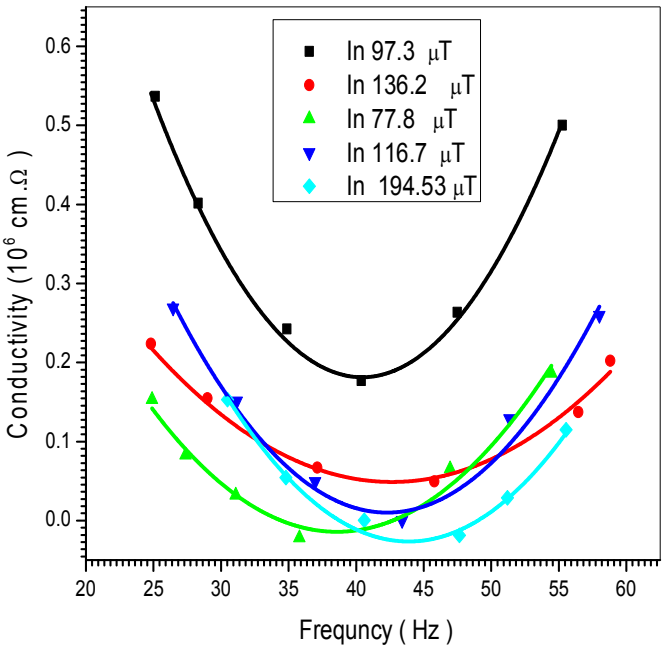

Fig (4.4.2) Relation between frequency (f) and Conductivity (σ)for different magneticflux densities for gold

Table (4.4.8) Relation between frequency (f) and magnetic field in different voltages

Frequency (Hz)	magnetic field(μT) In 400mV	magnetic field(μT) In 200mV	magnetic field(μT) In 180Mv
55.25746	194.53	96.73	90.94
47.48594	136.2	68.06	63.66
40.49329	116.7	58.33	54.6
35.4219	97.3	48.6	45
26.8109	77.8	38.9	36.4

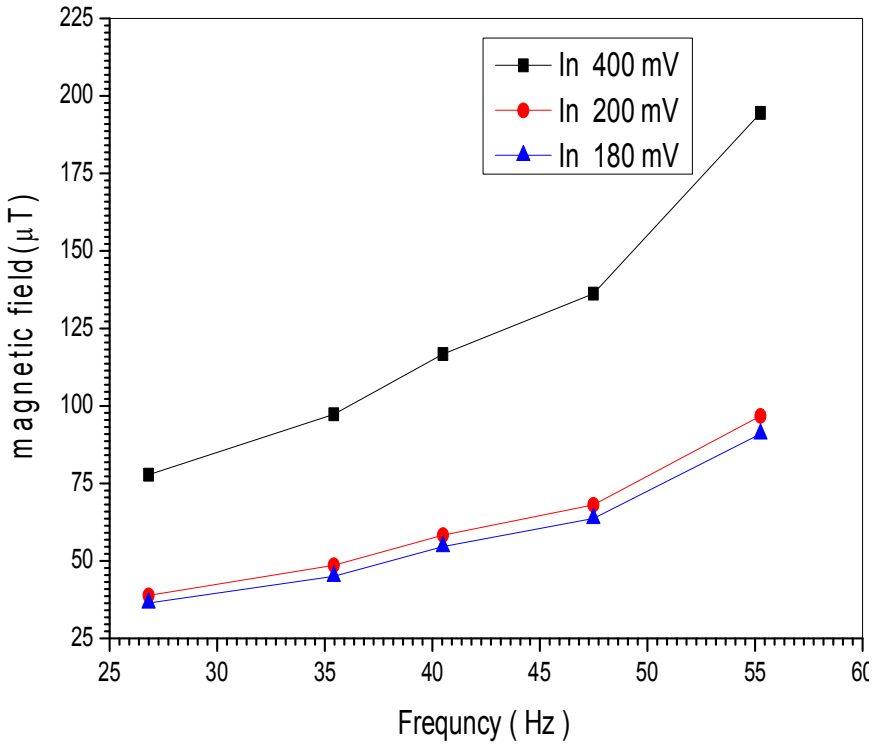

Fig (4.4.3) Relation between frequency (f) and magnetic field in different voltages

Table (4.4.9) Relation between frequency (f), Electron Affinity, Atomic number, and Density

Elements	Frequency (Hz)	ElectronAffinity (KJ/mole)	Atomicnumber(g /mole)	Density(kg/m^3)
Al	56	44.2	13	2700
Fe	29	16	26	7870
Sn	34	116	50	7300
Ag	50	112	47	8900
Au	24	223	79	19300
Cu	27	118	29	8960

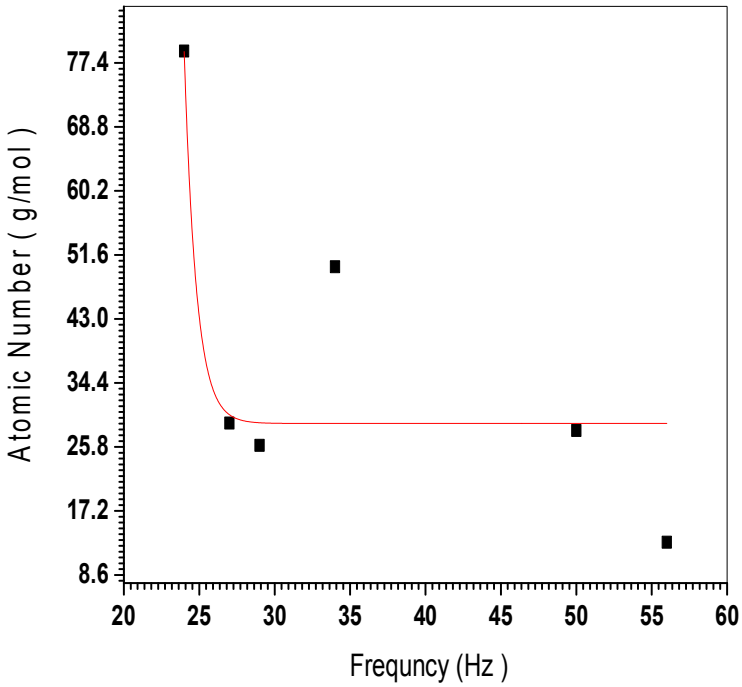

Fig (4.4.4) Relation between frequency and Atomic Number

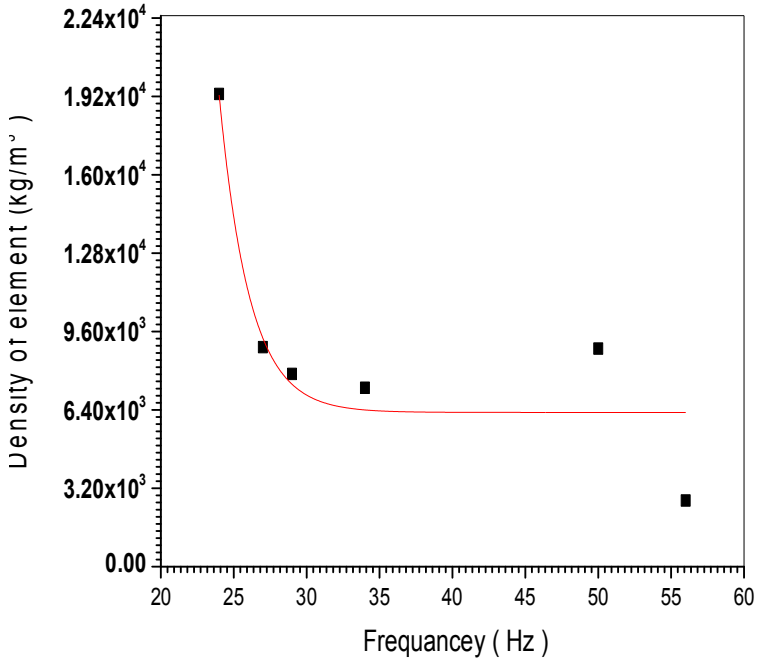

Fig (4.4.5) Relation between frequency and Density

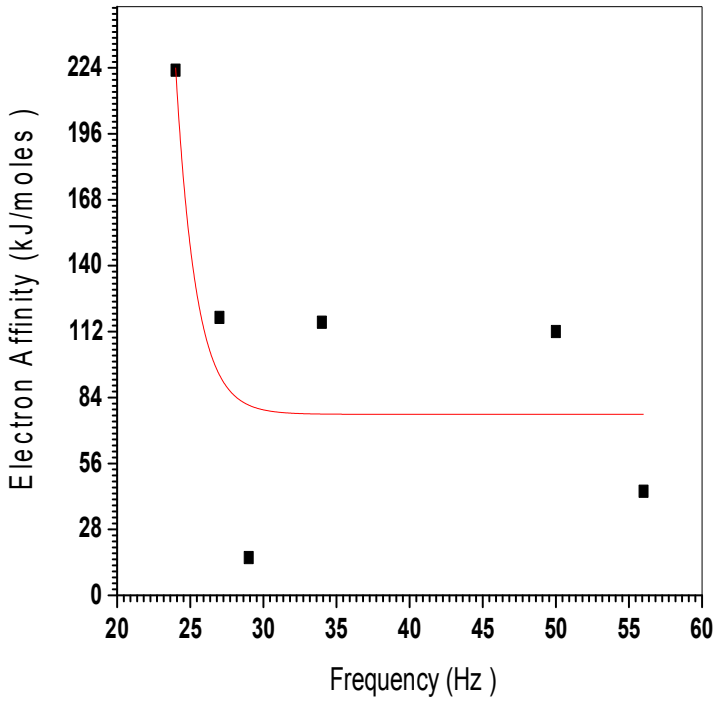

Fig (4.4.6) Relation between frequency and electron affinity

(4.5) Quantum Theoretical Model

Consider Klein – Gorden equation for a particle of rest mass m_o

$$\hbar^2 \frac{\partial^2 \psi}{\partial t^2} = -c^2 \hbar^2 \nabla^2 \psi + m_0{}^2 c^4 \psi \quad (4.5.1)$$

To separate variables Substitute wave function

$\psi = u(r)f(t)$ in (4.5.1) to get

$$-u\hbar^2 \frac{\partial^2 f}{\partial t^2} = -fc^2 \hbar^2 \nabla^2 u + m_0{}^2 c^4 fu \quad (4.5.2)$$

$$-\frac{1}{f}\hbar^2 \frac{\partial^2 f}{\partial t^2} = -\frac{1}{u}c^2 \hbar^2 \nabla^2 u + m_0{}^2 c^4 = E^2 \quad (4.5.3)$$

Where E represents the energy.

Therefore

$$-\frac{1}{f}\hbar^2 \frac{\partial^2 f}{\partial t^2} = E^2$$

$$\therefore -\hbar^2 \frac{\partial^2 f}{\partial t^2} = E^2 f \quad (4.5.4)$$

Where

$\hbar\omega_0$ =electron energy in bounded state.

$\hbar\omega$ = energy given to the electron.

$E = \hbar\omega - \hbar\omega_0$= excitation energy. (4.5.5)

Consider solution

$$f = \sin \alpha t \quad (4.5.6)$$

Inserting (4.5.6) in (4.5.5) yields

$$\hbar^2 \alpha^2 f = E^2 f \quad (4.5.7)$$

Thus

$$\hbar \alpha = E$$

In view of equation (4.5.5)

$$\alpha = \frac{E}{\hbar} = \omega - \omega_0 \quad (4.5.8)$$

Therefore the conductivity is given by

$$\because \sigma = \frac{ne^2\tau}{m} = \frac{|\psi^2| e^2 \tau}{m} = \frac{e^2\tau}{m} |\sin(\omega - \omega_0)t|^2 \quad (4.5.9)$$

Where the particles density n is related to the wave function ψ according to the relation

$$n = |\psi|^2$$

τ, e , m the symbols stand for relaxation time, charge, and mass respectively.

At near resonance $\omega - \omega_0 << 1$

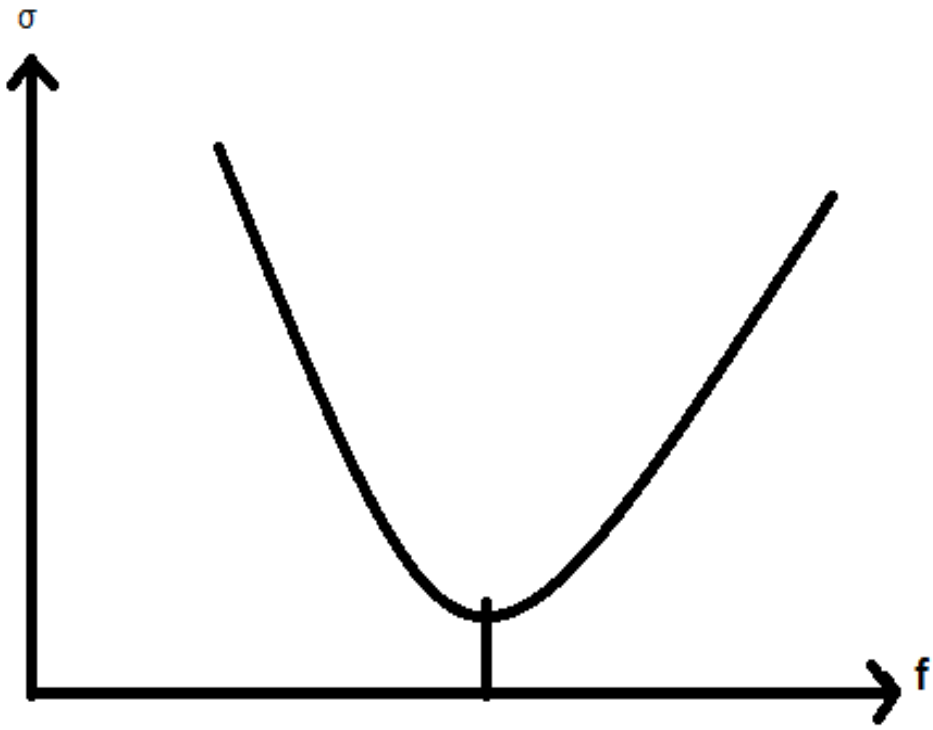

Fig (4.2) Theoretical relation between frequency (f) and Conductivity (σ)

$$\sin(\omega - \omega_0)t \approx (\omega - \omega_0)t \quad (4.5.10)$$

Inserting (4.5.10) in (4.5.9) yields

$$\therefore \sigma = \frac{e^2\tau}{m}t^2 \quad (4.5.11)$$

(4.5.1) Classical Absorption Conductivity Resonance Curve

Consider an electron of mass m oscillate with natural frequency ω_0.If an electric field of strength

$$E = E_0 e^{i\omega t} \quad (4.5.12)$$

Was applied, Then the equation of motion of the electron, in a frictional medium of friction coefficient γ, is given by

$$mx^{\bullet\bullet} = eE - m\omega_0{}^2 x - \gamma x^{\bullet} \quad (4.5.13)$$

Consider the solution

$$x = x_0 e^{i\omega t} \quad (4.5.14)$$

Thus

$$v = x^{\bullet} = i\omega x \qquad x^{\bullet\bullet} = -\omega^2 x \quad (4.5.15)$$

Interesting (4.5.14) and (4.5.15) and (4.5.12) in (4.5.13) yields

$$-m\omega^2 x = e\frac{E_0}{x_0}x - m\omega_0{}^2 x - \gamma v$$

Thus

$$v = -m\frac{(\omega^2 - \omega_0{}^2)}{\gamma}x + e\frac{E_0}{\gamma x_0}x \quad (4.5.16)$$

For simplicity consider large displacement amplitude x_0 compared to the electrical one E_0.Thus the last term in (4.5.16) can be neglected to get

$$v = -m\frac{(\omega^2 - \omega_0{}^2)}{\gamma}x \quad (4.5.17)$$

But the conductivity is given by

$$\sigma = \frac{e\tau}{m}n = \frac{e\tau}{m}n_0 e^{\frac{-\beta m v_e{}^2}{2}} \quad (4.5.18)$$

The number of photon is given according to the new statistical law as

$$n = n_o e^{\frac{E}{\overline{E}}} \quad (4.5.19)$$

Where the effective value v_e is related to the maximum value through the relation

$$v_e = \frac{v_0}{\sqrt{2}} \quad (4.5.20)$$

For small value of the power of e , one can expand exponential term to be

$$e^{-x} = 1 - x$$

Therefore equation (4.5.18) becomes

$$\sigma = \frac{e\tau}{m}n_0[1 + \frac{\beta m v^2}{4}] \quad (4.5.21)$$

Inserting (4.5.17) in (4.5.21) yields

$$\sigma = \frac{e\tau}{m}n_0[1 + \frac{\beta m^2 x_0{}^2(\omega - \omega_0)^2(\omega + \omega_0)^2}{4\gamma}]$$

$$\sigma = \frac{e\tau}{m} n_0 [1 + \frac{\beta m^2 \omega_0{}^2 x_0{}^2 (\omega - \omega_0)^2}{\gamma}] (4.5.22)$$

Where near resonance

$$\omega \approx \omega_0 \; \omega + \omega_0 \approx 2\omega_0 (4.5.23)$$

The relation between conductivity and frequency resembles that of (4.5.11) in its dependence on ω.

This relation is displayed graphically in Fig (4.2).

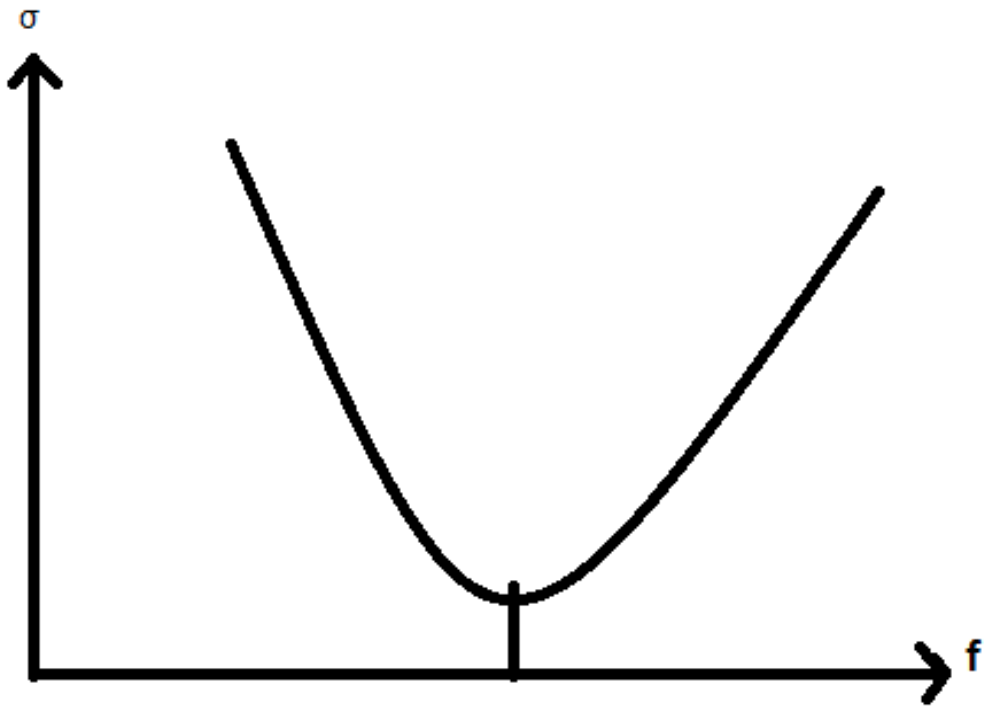

Fig (4.3) Theoretical relation between frequency (f) and Conductivity (σ)

(4.6) Discussion

The experimental work which was done shows variation of conductivity for gold according to Figs (4.4.1) and (4.4.2). The conductivity decreases then attains a minimum value in the range of (40-50 Hz), then increases a gain.

The theoretical expression (4.5.11) which is displayed graphically in Fig (4.2) is based on the ordinary expression for the conductivity. The electrons density n is found by solving Klein-Gordon equation for free particle. This is obvious as far as conduction electrons are free. The electron density is found from the square of the wave function, which is a sine function. Since at resonance ω is very near to ω_0, thus one can replace sin x by x (see equation(4.5.10)). The theoretical relation for f and σ obtained by this model resembles the experimental one in Fig (4.2).

Another classical approach based on Maxwell –Boltzmann distribution in section (3) shows a relation between σ and f in Fig (4.3) similar to experimental relation. The relations between σ and f resembles that of resonance, with minimum conductivity.

It is very interesting to note that each element has its own resonance conductivity at which conductivity is a minimum.In this model the ordinary expression for σ in eq_n (4.5.9) is used. But n here is found from Maxwell statistical distribution.

The emprical relation between applied magnetic field and resonance frequency resembles the theoretical one which shows exponential decay in fig (4.4.1).This confirms the relaibility of work done.

The emprical relation between resonance frequency on one hand with matter density, atomic number and electron affinity on the other hand which shows exponential decay as in figs (4.4.1), (4.4.2) and (4.4.3) can be explained also

on the basis of the statistical equation for non-equilibrium state as which shows relation between density and frequency theoreticallyFig (3.6.1).

The relation for atomic number Z is related to the fact that the number of free electrons n_f is proportional to the atomic number Z where

$$n_f \propto Z - n_b$$

Where

n_b is the number of bounded electrons.

(4.7) Conclusion

The experimental work done here shows that the conductivity changes with the frequency and have a minimum at a certain frequency, this frequency can be used to identify elements. Fortunately this experimental relation can be explained theoretically on the bases of Klein –Gordon equation or on the bases of Maxwell –Boltzmann distribution.

The empirical relation between resonance frequency of radiation and magnetic field obeys Zeeman Effect relation. The statistical distribution law based on plasma equation for non-equilibrium systems can describe the relation between matter density and atomic number on one hand and the resonance natural frequency of matter on the other hand.

(4.8) Suggested Future Work

We recommend further work in this area to use this simple technique for explorationand produce good metal detectors. This work utilizes simple technique based on electrical conductivity. We recommend further work to used simple electric circuitby simple components. The minimum frequency for each element, which can be used as a finger print characterizing itcould be further investigated as well. Other materials can be tested by the detector which releases conductivity and frequency.

References

[1]. M .A. Sons, Inc Quantitative Applications of Mass Spectrometry,Wiley & Sons, New York,(2000).

[2]. L. M. Schwartz, Anal. Chem, Nanofabricated optical antennas, (2011).

[3]. B. J. Millard, Quantitative Mass Spectrometry, Heiden, London, (2004).

[4]. D. A. Schoeller, Biomed. Mass Spectrum, New York, (1976).

[5]. rev. US EPA, Compounds in Water by Capillary Column Gas Chromatography – Mass Spectrometry, Cincinnati ,(1995).

[6]. M. Piehler J. A, specially applicable for mineralized soil with high sensitivity to gold and precious metals,Wiley, New York, (2010).

[7]. Saleh BEA, Teich. M.C., Fundamentals of photonics, Wiley, New York, (2007).

[8]. Grandin HM, Staedler B, Textor M, Vo¨ro¨s J ,Waveguide excitation fluorescence microscopy,(2006).

[9]. G. Chiba, High sensitive fluorescence spectrometer, Chim. Acta, (2008).

[10].Andrei Chtchedrine& Yuri Kolokolov, Frequency Meter Metal Detector, Circuit Cellar, May (2001).

[11].John Clarke, Fortune Finder, Silicon Chip, Dec (1999).

[12].Gavin Cheeseman, Metal Detectors (Part 2), Electronics and Beyond, June (1999).

[13].Popavic S. Grover and G. Moddel, "Engineering the current–voltage characteristics of metal–insulator–metal diodes using double-insulator tunnel barriers," Solid-State Electronics**,** (2012).

[14].Thomas and Rosa, "The Analysis and Design of Linear, Circuits," John Wiley & Sons, Inc., (2004).

[15].McGraw hill Encyclopedia of science and technology, 7th Ed, NY, (1992).

[16].Michael Plischke, BirgerBergersen, statistical physics, 3rd Edition, (2005).
[17].Demystified David McMahon, Quantum Mechanics, McGraw-Hill, New York, (1999).

[18].J. Burns, Solid State Physics (Academic press, Florida, (1985).

[19]. Charles Kittel, Introduction of Solid State Physics, (2003).

[20].Kasper Jensen Rene Jensen, Michael Nielsen, PI &LC.Osc Metal Detector, Analogue Project 1.SM, 1 December (2003).

[21]. Engineering Accreditation Commission, "Criteria for Accrediting Engineering Programs" (Accreditation Board for Engineering and Technology Inc), (1999).

[22]. Committee on Developments in the Science of Learning, How People Learn—Brain, Mind, Experience, andSchool, edited by John D. Bransford, Ann. L. Brown, and Rodney R. Cocking (National Academy Press, Washington, DC), (2000).

[23]. J.G. King, P. Morrison, and Ph. Morrison, "ZAP! Elementary experiments in electricity and magnetism: A progress report," *Am. J. Phys,* (1992).

[24]. Charles L. Garrett, Modern Metal Detectors (Ram Publishing Co., Dallas, TX), (2002).

[25]. Paul. A. Tipler, Physics for Scientists and Engineers, 4th ed. (W.H. Freeman), (1999).

[26]. Problem 6.4 in J.D. Jackson, Classical Electrodynamics, 2nd ed. (Wiley, New York), (1974).

[27] J. Zuloaga, E. Prodan and P. Nordlander, “Quantum description of the Plasmon resonances of a nanoparticle dimer,” Nano Lett, (2009).[28] J. Zuloaga, E. Prodan and P. Nordlander, “Quantum plasmonics: Optical properties and tenability of metallic nanorods,” ACS Nano (2010).
[29]D.C. Marinica, A.K. Kazansky, P. Nordlander, J. Aizpurua and A.G.Borisov, "Quantum plasmonics: nonlinear effects in the field enhancement of a plasmonicnanoparticle dimer." Nano Lett, (2012).
[30] R. Esteban, A.G. Borisov, P. Nordlander and J. Aizpurua, "Bridging quantum and classical plasmonics with a quantum-corrected model."NatureComm”, (2012).
[31] R. Alvarez-Puebla, L. M. Liz-Marzan and F. J. Garcia de Abajo, “Light concentration at the nanometer scale, J. Phys. Chem. Lett., (2010).
[32] W. Tantraporn, “Electron current through metal-insulator-metal sandwiches,” Solid-State Electronics,(1964).
[33] Modern Atomic and Nuclear Physics, C- Sharp Cook, VanNostrand, (1961).

[34] Physicals of atoms and molecules 2nd edition, (B.H. Brandsen and C.J. Joachaih, 1988 Pearson Education limited Essex CM20 2JE, Englend,(1988).

[35] Nuclear and Partical physic W E Burcbam and Jobes(1995,B.H.Brandsen and C.J. Joachaih, 1988 Pearson Education limited Essex CM20 2JE,Englend,(1988).

[36] B .H .Bransden& G. J .Joachim, Quantum Mechanics, second edition, England, (2000).

[37] D. H. Sandiford, A .G .Phillips, Introduction to Quantum Mechanics, Wiley, (2010).

[39] P. M Mathews, K. Venkatesan ,Atextbook of Quantum Mechanics, New Delhi,(2007).

[40] Nuclear and Particle Physics, .B. R. Martin, John Wiley & Sons, Ltd (2006).

[41] The atom ,6th edition SIRGEORGE Thomson,Oxford university press Amentouse, London,E.c.4,(1962).

[42] Modern physics, 3th Edition STEPHEN T.THORNTTON and ANDREW REX , Thomson learning Academic resource center , Canada,(2006).

[43]RADIATION ONCOLOGY PHYSICS: A HANDBOOK FORTEACHERS and STUDENTS, INTERNATIONAL ATOMIC ENERGY AGENCY VIENNA, (2005).

[44] Blatt, Frank J, Modern Physics, McGraw Hill, (1992).

[45] Evans, Robley D., The Atomic Nucleus, McGraw-Hill, (1955).

[46] Halliday, Resnick and Walker, Fundamentals of Physics, 4th Edition, Extended, Wiley ,(1993).

[47] Tipler, Paul A. and Llewellyn, Ralph A., Modern Physics, 3rd Ed., W.H. Freeman, (1999).

[48] Serway, Raymond, Moses, Clement and Moyer, Curt, Modern Physics, Saunders College Publishing, (1989).

[49] Rohlf, James William, Modern Physics from a to Z0, Wiley, (1994).

[50] Tipler, Paul, Physics for Scientists and Engineers, Extended, Worth, (1991).

[51] Serway, Raymond A, Physics for Scientists and Engineers with Modern Physics, 3rd Ed, Saunders, (1990).

[52] Atomic Physics, Max Born ,Blackle and Son Iimited, London and Glasgow,(1937).

[53] Basic Physics of Nuclear Medicine, Kieran Moler ,Wikibooks(2006).

[54] Modern Atomic and Nuclear Physics, C. Sharp Cook , Van No strand (1961).

[55]Models of the Atomic Nucleus ,N.D. Cook (2nd ed.), Springer.pp. xvi& 324. (2010).

[56] Garrett, Charles, "The New Modern Metal Detectors,"Garrett Books, 1996.

[57] Physics to Daily Life: Applications in Biology, Medicine, and Healthcare, Beatrice Bressan , Wiley-Blackwell, (September 2014).

[58]A .Beiser .concept of modern Physics ,Mc Hill company ,New York ,(1990)

[59] John S. Townsend, A Modern Approach to Quantum Mechanics ,

United states of America ,Unversity Science Books,(2000).

[60] Walter Greiner, Quantum Mechanics: An Introduction, New York ,Springer Science & Business Media, (2001).

[61]Ashok Das & Adrian C. Melissinos ,Quantum Mechanics: A Modern Introduction, New York, (1986).

[62] D .law &G.Fetzer ,s .Mesropian ,Quantum interference of large organic molecules ,Nature . com .Retrieeved(2013).

[63]Popavic, "Introduction of Electromagnetics,"Prentice Hall, 2000.

[64]W .C .Schieve and L . P. Horwitz ,Quantum Statistical Mechanics, Cambridge University press , New York ,(2009) .

[65]MSSL, BASICS OF SPECTROSCOPY, Spectroscopy School,FritsPaerels, Columbia Astrophysics Laboratory,Columbia University, New York, (2009).

[66] Electromagnetism, Addison Wesley Pollack, Gerald L, Stump, Daniel R. (2002).

[67] Swasan A. Elhuri , M. Dirar , Quantization of friction Nano Isolated system , Elixir Condensed Matted Physics, Vol .81,PP 31430-31435 (2015).

[68] K.G. Elgaylani, M. Diraretal , Derivation of Klein-Gordon Equation from Maxwells Equation, International J- of Physical sciences , vol. 2 ,PP 015-020, feb (2014).

[69] Rehab Ibrahim HamadEisa , M. Dirar ,Interpretation of the change of Intensity and Spectral line width for Bhutan, Neon, Fluorine, and Chlorine by Using Complex Statistical Distribution and Quantum harmonic Oscillator Model (IOSR Journal of Applied Physics (IOSR-JAP), e-ISSN: 2278-4861.Volume 7, Issue 3 Ver. II (May. - Jun. 2015).

[70] Duane Liedahl, The X-Ray Spectral Properties of Photo ionized Plasma andTransient Plasmas, in X-ray Spectroscopy in Astrophysics, Lecture Notes in Physics, (Springer, 1999).

[71] Rehab Ibrahim HamadEisa, M. Dirar, Explanation of Intensity Spectral change of Bhutan, Carbon dioxide , Carbon Monoxide, Oxygen, Nitrogen Gases on the basic of Nun Equilibrium (IOSR Journal of Applied Physics (IOSR-JAP), e-ISSN: 2278-4861.Volume 7, Issue 3 Ver. II (May - Jun 2015).

[72] Suhair S. MakawySuleiman,PhD Thesis,Derivation of Statistical Distributions for non -Thermally Equilibrium Systems,Sudan University of Science and Technology,Khartoum,(2012).